Volume 35, Number 01

In this Issue

Generalized Stefan-Boltzmann Law: A tutorial

Debnarayan Jana

Department of Physics

University of Calcutta

92 A P C Road, Kolkata- 700009, India.

djphy@caluniv.ac.in

Abstract

In this article, we would like to discuss the implications of Stefan-Botzmann law in blackbody radiation in an arbitrary spatial dimensions d with power law dispersion relation. After the classical derivation of Stefans law in an arbitrary diemsion, we critically indicate the role of dimensional analysis in determing the unknown integration constant. Subsequently the quantum derivation rightly points out the diversity associated with the law in dealing the mixed spectrum for computing density of states and effective number of particles in a given temperature. This approach clearly indicates the distinction between massless (ultra-relativistic) photons and massive (non-relativistic) particles. As a part of the tutorial, few problems are added with solutions to check the concepts.

Keywords: Black Body Radiation, Planck's law, Stefan-Boltzmann Law.

1.Introduction

The concept of black body radiation along with Planck's radiation, Stefan's law and Wiens displacement law forms an integral part of the undergraduate and post-graduate classes. These laws are important in predicting the temperature of cosmic background radiation, any thermal source and the color of the star.

Before we start, it is necessary to understand the meaning of black body radiation [1, 2, 3, 4] as there are confusions in several text books. For a historical look into this law, the readers are referred to documents [5, 6, 7]. The radiation law has also been viewed from dimensional analysis [8, 9, 10, 11, 12]. The most well used Planck's contant in quantum mechanics can be determined from the experiments related to black body radiation [13, 14, 15, 16]. In figure 1, we show some examples of blackbody radiation. In modern physics,

the physics at the Planck scale [17] and the contrasting role of Plancks constant [18] seem to be very exciting.
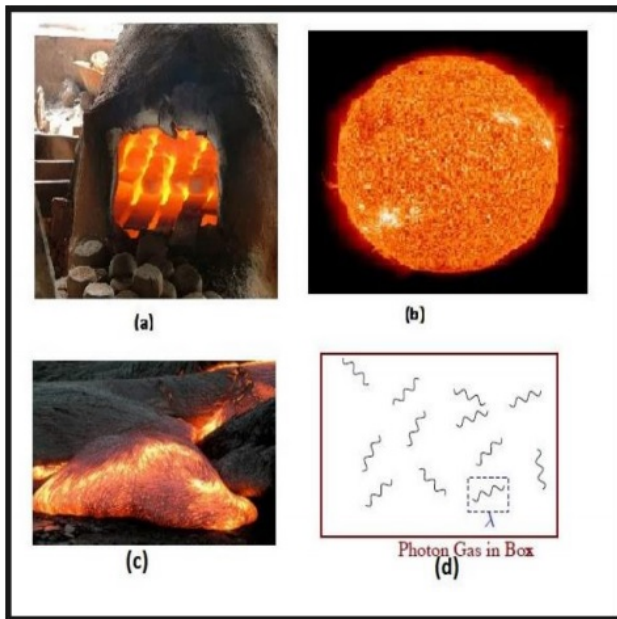
Figure 1: Examples of Blackbody Radiation. (a) An Oven (b) Sun (c) Volcano -real life Black Body and (d) Theoretical Physicists Black body. Source: $http$: $//tonic.physics.sunysb.edu/ dteaney/ F12 mystery$

Most of the book starts with the perfectly black an idealized rather than the simple black body one. A black body is a body in thermal equlibrium with the surroundings and can absorb and emit electromagnetic radiation at all frequencies regardless of angle of incidence with a characteristic continuous emission spectra satisfying Planck's radiation formula. An emitting blackbody with *shorter* wavelengths have *higher* intensity ra- diation (and greater energy flux) than the *longer* wavelength. A

perfectly black body is an idealized concept which allows all incident radiation to pass into it and internally absorbs all the incident radiation. Therefore, for a perfectly black body there is no reflection or transmission of electromagnetic rediation. Therfore, the perfect black body is indeed a perfect absorber for all incident radiation as well as for all angles of incidence. In fact, the term black body was intro- duced by Gustav Kirchhoff in 1860. Because no light (visible electromagnetic radiations) is reflected or transmitted, the object appears black when it is cold. Therfore, the perfect black body is indeed a perfect absorber for all incident radiation as well as for all angles of incidence. A black body emits temperature dependent spectrum of light.

An approximate realization of a black body is thought of a system having a hole in the wall of a large enclosure. In figure 2, we depict the typical black body radiation spectra as a function of wavelength.

At room temperature, black bodies emit mostly infrared light, but as the temperature increases past a few hundred degree centigrade, it is observed that they start to emit visible wavelengths, from red, through or- ange, yellow, and white before ending up at blue. This change in color is indicative of the fact that the frequency distribution of the emitted radiation changes with temper- ature. This is due to Wiens displacment law [19] states that an increase of temperature in an object not only increases the

total ra- diant output, but also shifts this energy out- put to shorter wavelengths, in inverse propor- tion to the absolute temperature.
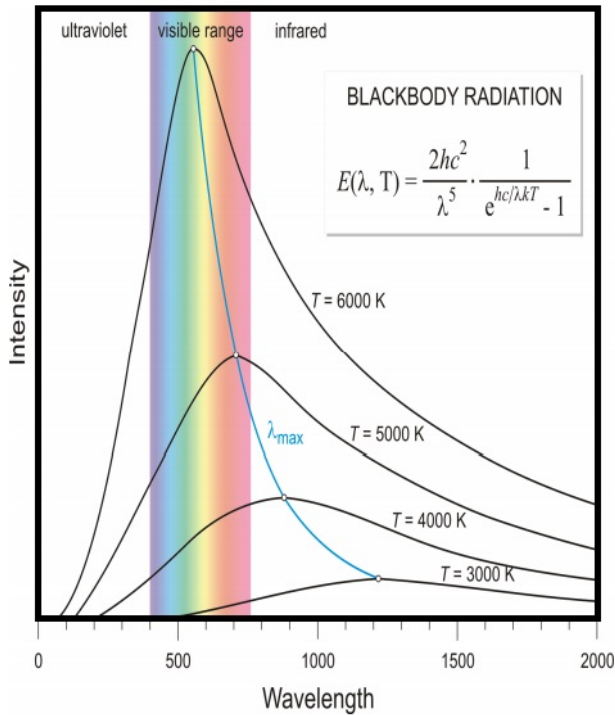
Figure 2: Typical spectrum of blackbody radiation as a function of wavelength. Source: $https://en.wikipedia.org/wiki/Blackbody\ radiation$

If one slowly and steadily increases the temperature of a material body, it is observed that the predominant color shifts from dull red through bright yellow-orange to bluish white heat. This change in color is indicative of the fact that the frequency distribution of the emitted radiation changes with temperature. The typical black body radiation spectra as a function of frequency is shown in figure 3 .

Since the thermal radiation spectrum strongly depends on temperature, the tem-
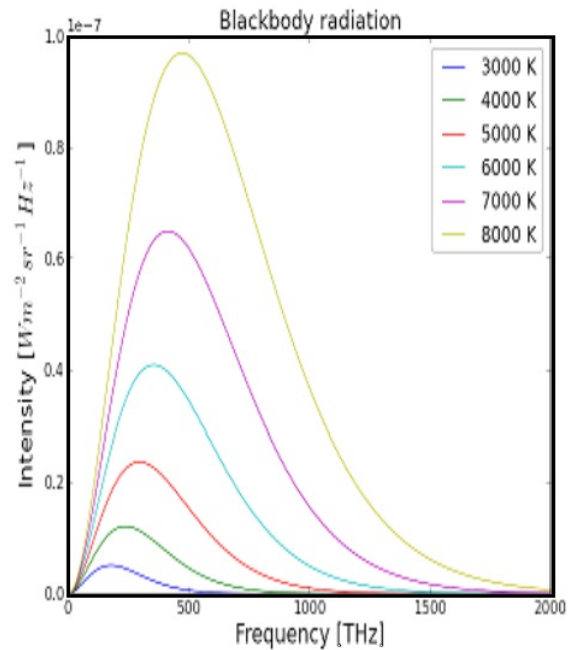
Figure 3: Typical relationship between the temperature of an object and the spectrum of blackbody radiation it emits as a function of frequency. Source: $https://energyeducation.ca/encyclopedia$

perature of a hot body through the emitted radiation can be estimated from this. Thus, it seems that a blackbody can capture an essential aspect of the radiation from a real body like the visible glow from a lump of iron at $1000°$ C, to the Sun at $6000°$ C or even the invisible infrared faint glow of a human body at $37°$ C. As a consequence, the solar radiation is concentrated in the ultra-violet (UV), visible and near infrared regions of the spectrum, while radiation emitted by planets and their atmospheres is largely confined to the infrared regime. We can distinguish between solar and terrestrial radiation, using Planck's Law and Wien's

Law. Since, the surface temperature of Sun is higher than that of Earth, the radiation spectra of Sun is peaked at shorter wavelength (higher energy) regime while that of Earth at longer wavelength (lower energy). In figure 4, we compare the blackbody radiation spectrum of the Sun and Earth in the same graph. It is to be noted that at normal Earth temperatures, the thermal emission is in infrared regime. An order of magnitude of $\frac{hc}{k_B}$ can be estimated from the visible solar spectrum radiation. using the blackbody spectrum [20].

This automatically brings about the notion about a white body. Accordingly, a white body is one having a rough surface reflecting all incident rays completely and uniformly in all directions. In this situation one should remember that the radiation from light emitting from LASER does not satisfy the features of black body radiation.

Thus, the definition clearly establishes the fact that it is indeed a phenomenon from equilibrium statistical mechanics. The spectrum of such a body depends only on the temperature rather than the shape or composition of a body. Stefan Boltzmanns law [21, 22] is connected with the radiation of a black body need not be perfectly one. The total radiant energy (E) per second per unit area of the surface of a black body is directly proportional to the fourth power of its absolute temperature. Mathematically speaking,
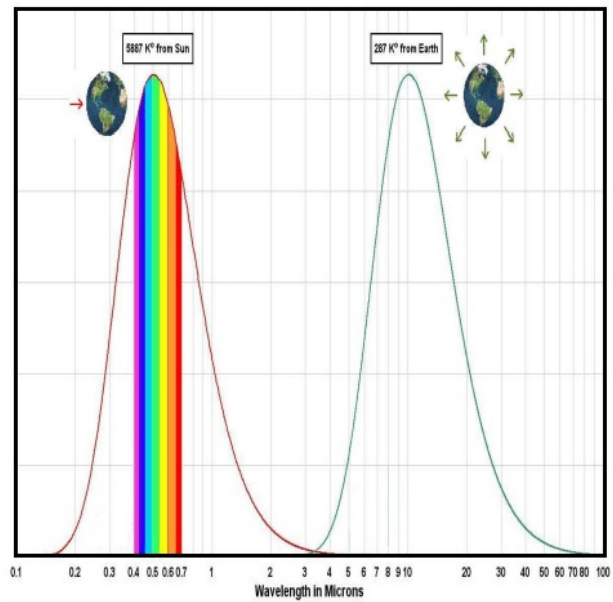
Figure 4: Blackbody radiation Sun and Earth as a function of wavelength. Source: $http://www.planetforlife.com/greenexplainSpectra$.

$$E = \sigma T^4, \qquad \sigma = \frac{2\pi^5 k_B^4}{15c^2 h^3} \qquad (1)$$

σ is a constant better known as Stefan's constant [23] equal to 5.67×10^8 W m^2 K^4. The numerical dimensionless factors appearing in the above equation however vary (such as $\frac{\pi^4 k_B^4}{60c^2 h^3}$ power raiated by surface element of black body) depending on the various ways of definitions, however, the dependences on two fundamental constants (k_B and $\hbar$) remain intact. If a surface emits radiation with a known flux density, then the above equation can be used to solve for its equivalent blackbody temperature, that is, the temperature a blackbody would need to have in order to emit the same flux density of radiation. In the most simplified case, if the surface emits as a blackbody, its ac-

tual temperature and its equivalent black-body temperature will be the same.

The fact that it is proportional to T^4 is purely classical. This law has been verified extensively via incandescent light bulb in laboratory [24, 25, 26, 27, 28, 29, 30, 31, 32]. However, the value of the proportionality constant σ requires quantum mechanics. This power law dependence can be understood physically from the relevant active modes. The "active" modes in a system are those modes where the energy required for exciting those modes at a given temperature T is less than $k_B T$ by the equaipartition theorem. If the energy is more than, the energy stored in those modes is suppressed according to Boltzmann distribution. Thus, in these active modes, there is roughly $k_B\mathrm{T}$ amount of energy. Besides, these modes characterized by momenta stay inside a sphere of radius proprtional to $k_B\mathrm{T}$. Now, since, the volume of this sphere is proprtional to T^3, we obtain the total energy of these modes as T^4. Generalizing to an arbitrary spatical dimension d, we get T^{d+1}. This intutitive argument leads to the fact that the low temperature specific heat of solid (lattice part) according to Debye model as T^d. One should also note that there is no physical infinite specific heat for an equilibrium radiation [33]. In such a situation it is the pressure which is solely function of temperature T and the derivative $\left(\frac{\partial P}{\partial T}\right)$ (P being the pressure) only meaningful quantity. Thus to summarize, we indicate below the main charcteristic features of back body ra-

diation.

- Radiation emitted by a blackbody is isotropic, homogeneous and unpolarized.

- Blackbody radiation at a given wavelength depends only on temperature.

- Any two blackbodies at the same temperature emit precisely the same radiation.

- Finally, a blackbody emits more radiation than any other type of an object at the same temperature.

- It is the Planck function which gives the intensity (or radiance) emitted by a blackbody having a given temperature.

- Blackbody radiant intensity increases with temperature.

- Lastly but not the least, the wavelength of maximum intensity decreases with in- creasing temperature.

In fact, Planck function relates the emit- ted monochromatic intensity to the frequency and the temperature of the emitting substance.

2. Review of "classical" derivation of SB law

We start with the basic thermodynamic relations by assuming the internal energy U as a state function of volume V and temperature

T. Using first and second law of thermodynamics, we can write

$$dU = dQ - PdV = TdS - PdV \qquad (2)$$

Again by assuming, the entropy S as a state function of V and T, we can write

$$dS = \left(\frac{\partial S}{\partial T}\right)_V dT + \left(\frac{\partial S}{\partial V}\right)_T dV$$

$$\begin{aligned} dS &= \left(\frac{\partial S}{\partial T}\right)_V dT + \left(\frac{\partial S}{\partial V}\right)_T dV \\ &= \frac{c_V dT}{T} + \left(\frac{\partial S}{\partial T}\right)_V dV \end{aligned} \qquad (3)$$

The second term in the second line follows from Maxwells relation. Substituting this equation (3) for entropy in the equation (2), it is easy to see that

$$dU = c_V dT + \left[T\left(\frac{\partial P}{\partial T}\right)_V - P\right]dV \qquad (4)$$

From the above equation (4), it follows immediately that,

$$\left(\frac{\partial U}{\partial V}\right)_T = \left[T\left(\frac{\partial P}{\partial T}\right)_V - P\right] \qquad (5)$$

For an ideal gas ($PV = RT$) whether it is non-relativistic or ultra-relatibistic, $\left(\frac{\partial U}{\partial V}\right)_T = 0$. Physically speaking, a change in volume of the container of the gas particles eventually changes the average distance between the particles. As a result, the average potential energy changes which depends on the distance via the volume of

the container. the average potential energy is either constant or zero (independent of distance). Thus, the internal energy of an ideal gas is independent of volume. Thus, a non-zero value of $\left(\frac{\partial U}{\partial V}\right)_T$ can be regarded as the hallmark of interaction between the particles.

For a hypothetical dispersion relation of photons as $\omega \sim k^s$ in an arbitrary spatial dimension d, it is easy to understand that the internal energy $U \sim \frac{1}{V^{s/d}}$. As a result, the radiation pressure can be written as $P = \frac{s}{d}\frac{U}{V}$. For ideal gas using $PV = Nk_B T$, we find

$$U = \frac{d}{s}NK_B T \qquad (6)$$

Now, with the help of equation (5) and defining the energy density $u = \frac{U}{V}$, we get

$$\begin{aligned} \frac{d}{s}P &= \frac{s}{d}T\frac{\partial u}{\partial T} - \frac{s}{d}u \\ \frac{du}{u} &= \frac{d+s}{s}\frac{dT}{T} \\ u &= K_d T^{\frac{d+s}{s}} \end{aligned} \qquad (7)$$

The (integration) constant K_d cannot be evaluated through this classical way of deriving the above generalized Stefans law ($d = 3, s = 1, u \propto T^4$) but its dependence on the fundamental physical constants can be understood from simple dimensional analysis [34]. It is instructive to notice that for a massive bosons with quadratic dispersion ($s = 2$), $u \propto T^{5/2}$ in agreement with kinetic theory because $p = \frac{2}{3}u$. Without using equation (5) it is possible to derive Stefans law

from thermodynamics as follows. From conservation of energy (first law +second law) we can write

$$TdS = d(uV) + PdV$$
$$= V\left(\frac{\partial U}{\partial T}\right)dT + \left(\frac{d+s}{d}\right)udV$$

(8)

In passing, we note that the derivatives of the entropy function are:

$$\left(\frac{\partial S}{\partial T}\right)_V = \frac{V}{T}\frac{du}{dT} \qquad \left(\frac{\partial S}{\partial V}\right)_T = \frac{d+s}{d}\frac{u}{T}$$

(9)

Again, entropy being a state function of volume V and temperature T and exact differential, hence, it is path-independent and satifies the relation

$$\left(\frac{\partial^2 S}{\partial V \partial T}\right) = \left(\frac{\partial^2 S}{\partial T \partial V}\right)$$

(10)

As a consequence, we obtain the final equation as

$$\frac{1}{T}\frac{du}{dT} = \left(\frac{d+s}{d}\right)\left(T\frac{du}{dT} - u\right)\frac{1}{T^2}$$

(11)

which after integration yields the equation (7). In fact, this is the way Boltzmann derived T^4 law from pure thermodynamics. The constant K$_d$ can be obtained from dimensional analysis by assuming the energy density depends on three fundamental constants Boltzmann constant k$_B$, Planck's constant $\hbar$ and the speed of light c. Therefore, we can write for s = 1 (linear dispersion for massless photons)

$$\frac{ML^2T^{-2}}{L^d} = c^x\hbar^y(k_BT)^z$$

(12)

Equating the powers of M, L and T, we obtain the energy density u as

$$u(T,d) \propto \frac{1}{(\hbar c)^d}(k_BT)^{1+d}$$

(13)

Instead of energy density, if one looks into the process of radiation then it is revealed that the intensity of radiation I(d, T) (power falling per unit area) depends essentially on three fundamental physical constants namely Boltzmann constant k$_B$, Planck's constant $\hbar$ and the speed of light c. Therefore, from dimensional analysis it is clear that

$$\frac{ML^2T^{-3}}{L^{d-1}} = c^x\hbar^y(k_BT)^z$$

(14)

Therefore, equating the powers of M, L and T, we get $x = 1 - d$, $y = -d$ and $z = 1 + d$. The scaling form (without the dimensionless constant) of Stefan's law from the consideration of intensity in an arbitrary spatial dimension is given by

$$I(d,T) = \frac{k_B^{d+1}}{\hbar^d c^{d-1}}T^{d+1}$$

(15)

The interesting point is that we can relate Stefan's constant (without the dimensionless numbers) from simple dimensional analysis in an arbitrary spatial dimension d as

$$\sigma(d) = \frac{k_B^{d+1}}{\hbar^d c^{d-1}}$$

(16)

It is interesting to point out that for $d = 1$ and $\omega = ck$, the energy density $u \approx$

$\frac{(k_B T)^2}{\hbar c}$ is reminiscent of characteristic feature of quantum system in one dimension such as free fermions at finite density, Luttinger liquid, quantum Hall edge states and many critical quantum spin chains. A formal dimensional analysis important for finite mass system can be obtained as follows; the energy density instead of the speed of light depends on the mass of the particles. Therefore, the equation (14) reduces for s = 2 in such a situation

$$\frac{ML^2T^{-2}}{L^d} = m^x \hbar^y (k_B T)^z \qquad (17)$$

Equating the powers of M, L and T, we obtain the energy density u as

$$u(m, T, d) \propto \frac{m^{\frac{d}{2}}}{\hbar^d} (k_B T)^{(1+\frac{d}{2})} \qquad (18)$$

In particular for $d = 3$, the above equation (18) reduces for massive particles [35] as

$$u(m, T) \propto \frac{m^{\frac{3}{2}}}{\hbar^3} (k_B T)^{5/2} \qquad (19)$$

and is the typical energy density for Bose-Einstein condensation or the 3d ferrmagnetic magnon energy density, From both the situations, one obtains the low temperature specific heat proportional to $T^{3/2}$. In the magnon case, this variation of specific heat is known as Bloch's $T^{3/2}$ law. Now combining equations (13) and (18), we can generalize Stefan-Boltzmann law [35] for massive particles in d$_m$ dimensions and massless photons in d$_c$ as

$$u(T) = \frac{(mc^2)^{\frac{d_m}{2}}}{(\hbar c)^{d_c + d_m}} (k_B T)^{1 + d_c + \frac{d_m}{2}} \qquad (20)$$

A compactification of the above formula follows if one replaces $d_0 = d_c + d_m$ and $\gamma = d_c + \frac{d_m}{2}$

$$u(T) = \frac{(mc^2)^{d_0 - \gamma}}{(\hbar c)^{d_0}} (k_B T)^{1+\gamma} \qquad (21)$$

The exact form (through incorporation of some dimensionless constants) can be obtained from the quantum derivation of this law. Some other related thermodynamic relations can be addressed from the above generalized Stefan's law. Using the second law of thermodynamics, we get

$$TdS = Vdu + u\left(1 + \frac{s}{d}\right)dV \qquad (22)$$

Using $u = \sigma(d, s) T^{1+\frac{d}{s}}$ and integrating, we find the entropy as

$$S = \sigma(d, s) V\left(1 + \frac{s}{d}\right) T^{\frac{d}{s}} \qquad (23)$$

Again, for an adiabatic change ($dQ = 0$), the similar analysis yields

$$\left(1 + \frac{s}{d}\right)udV + Vdu = 0$$

$$VT^{\frac{d}{s}} = constant \qquad (24)$$

In otherwords, for an enclosure of radius R in an arbitrary spatial dimension d, we get

$$RT^{\frac{1}{s}} = K_1 \qquad (25)$$

with the fact that the constant K_1 depends on the spatial dimension d. Before we end this section one comment is in order. Within classical electromagnetic theory. Boyer [36] has established that the presence of Lorentz invariant classical electromagnetic zero-point radiation can explain the Planck blackbody spectrum.

3. Review of "quantum" derivation of SB law

The canonical partition function for phontons in state k and polarization ϵ with dispersion $\omega \sim k^s \sim V^{-\frac{s}{d}}$ is given by

$$Q = \prod_{k,\epsilon} \frac{1}{1 - e^{-\beta\hbar\omega}} \qquad (26)$$

Assuming two directions of polarization, the internal energy can be computed as

$$U = -\frac{\partial logQ}{\partial \beta}$$
$$= \sum_k \hbar\omega <n_k> \qquad (27)$$

with $<n_k> = \frac{2}{e^{\beta\hbar\omega}-1}$. It is easy to visualize the pressure P as

$$P = \frac{1}{\beta}\frac{\partial logQ}{\partial V} = \frac{s}{d}U \qquad (28)$$

In the thermodynamic limit in an arbitrary spatial dimension d, we can write the internal energy as

$$U = \frac{2V\pi^{\frac{d}{2}}}{(2\pi)^d\Gamma(\frac{d}{2}+1))} \int_0^\infty \frac{k^{d-1}\hbar ck^s dk}{e^{\beta\hbar ck^s}-1} \qquad (29)$$

A simple scaling analysis yields $U/V \sim T^{1+\frac{d}{s}}$ and the energy density (generalized Planck's law) can be obtained [37] as

$$u(d,\omega,T) = \frac{2\hbar\pi^{d/2}}{(2\pi)^d\Gamma(\frac{d}{2}+1)c^{d/s}}\frac{\omega^{d/s}}{e^{\beta\hbar\omega}-1} \qquad (30)$$

A cross-check for Planck's radiation law is done with $d=3$ and $s=1$ as

$$u(\omega,T) = \frac{\hbar}{\pi^2c^3}\frac{\omega^3}{e^{\beta\hbar\omega}-1} \qquad (31)$$

For a small finite zero rest mass, instead of two directions of polarization, there will be three directions and hence, the equation (31) is modified accordingly

$$u(\omega,T) = \frac{3\hbar}{2\pi^2c^3}\frac{\omega^3}{e^{\beta\hbar\omega}-1} \qquad (32)$$

However, it should be noted that in both cases, the average energy density will be proportional to fourth power of the absolute temperature. Using $\omega = \frac{c}{\lambda}$ we get the generalized Wien's distribution from equation (30) as

$$u(d,\lambda,T) = \frac{2\hbar\pi^{d/2}}{(2\pi)^d\Gamma(\frac{d}{2}+1)}\frac{c}{\lambda^{2+\frac{d}{s}}}\frac{1}{e^{\beta\hbar\omega}-1} \qquad (33)$$

with the scaling law as

$$u(d,\lambda,T) = \frac{f(\lambda T)}{\lambda^{2+\frac{d}{s}}} \qquad (34)$$

As a further extension we can establish the generalized Wien's displacement law [19, 38]($\lambda_{max}T = g_d(constant)$) by solving the transcendental equation

$$\frac{x}{2 + \frac{d}{s}} = 1 - e^{-x}$$

$$e^x \left(1 - \frac{x}{2 + \frac{d}{s}} \right) = 1 \tag{35}$$

consistent with the form derived for an arbitrary dimension in $s = 1$ case [39]. One can also compute an equivalent Wien's displacement law from the average photon energy [7]. The average photon energy in an arbitrary dimension d is defined as

$$\bar{E} = \frac{\int_0^\infty u(d, \omega, T) d\omega}{\int_0^\infty \frac{u(d, \omega, T)}{\hbar \omega} d\omega} \tag{36}$$

A simple scaling relation indicates that the denominator is proportional to $T^{\frac{d}{s}}$ while the numerator to $T^{\frac{d}{s}+1}$. As a result, the average photon energy is proportional to T. Based on this, we can associate a wavelength satisfying the relation

$$\lambda_{\bar{E}} T = constant \tag{37}$$

independent of both d and s. Using the dimensionless variable $x = \frac{h\nu}{k_B T} = \frac{hc}{\lambda k_B T}$, we can rewrite the Planck's radiation distribution as

$$u(x) = 2ck_B \left(\frac{k_B}{\hbar c} \right)^{\frac{d}{s}} T^{\frac{d}{s}+1} \frac{x^{\frac{d}{s}+1}}{exp(x) - 1} \tag{38}$$

In the limiting case of $d = 3$ and $s = 1$, it correctly reproduces the equation as suggested by the authors of the ref [7]

$$u(x) = \frac{2(k_B T)^4}{\hbar^3 c^2} \frac{x^4}{exp(x) - 1} \tag{39}$$

Thus, it is clear from the above discussion that Stefan-Boltzmann law is not a classical but a quantum due to the appearance of as Planck's constant $\hbar$ in the denominator of the law. Moreover, it is also noticed that the energy density diverges as $\hbar$ approaches zero.

4. Integrated Density of States and number of particles

The density of states $g(E)$ is defined as the number of states lying within an energy interval E and $E + dE$ in a unit volume. For a dispersion relation of the form $E \sim k^s$, it is easy to verify that the density of states $g(E) \sim E^{\frac{d}{s}-1}$. The integrated density of states counts the number of particles in a given interval E_0 as $N(E_0) = \int_0^{E_0} dE \, g(E)$, assuming that the $g(E) = 0$ at $E = 0$. In this language, the average energy of the system can be defined as

$$U(T) = \int_0^{k_B T} E \, g(E) dE \tag{40}$$

Inserting, the power law variation of g(E) with E, we obtain $U(T) \sim T^{\frac{d}{s}+1}$ consistent with generalized Stefan-Boltzmann law. In this scenario, the number of particles $N(T)$ at a given temperature can be written as $N(T) = \int_0^{k_B T} g(E) \, dE \sim (k_B T)^{\frac{d}{s}}$. More explicitly, for linear dispersion $E = \hbar kc$ in any arbitrary dimension d, it can be easily visualized that

$$g(E) \sim \frac{E^{d-1}}{(\hbar c)^d} \qquad N(T) \sim \frac{(k_B T)^d}{(\hbar c)^d} \tag{41}$$

In particular for $d = 2$, the graphene monolayer does indeed satisfy $N(T) \sim \left(\frac{k_B T}{\hbar c}\right)^2$ with $U(T) \sim T^3$ giving rise to $C_v \sim T^2$. On the otherhand for quadratic dispersion such as $E = \frac{\hbar^2 k^2}{2m}$ we find in an arbitrary spatial dimension d

$$g(E) \sim \frac{m^{d/2}}{\hbar^d} E^{\frac{d}{2}-1} \quad N(T) \sim \frac{m^{d/2}}{\hbar^d} (k_B T)^{\frac{d}{2}} \tag{42}$$

As a consequence, for $d = 2$ the graphene bilayer satisfies $N(T) \sim \frac{m}{\hbar^2}(k_B T)$ with $U(T) \sim T^2$ giving rise to linear variation of specific heat with temperature. This kind of analysis also can be applied to some hypothetical mixed/ hybrid system where both linear as well as quadratic dispersion relation appear in the following fashion [35]

$$E = \sqrt{\left(\frac{\hbar^2 k_x^2}{2m}\right)^2 + \hbar^2 k_y^2 c^2} \tag{43}$$

In a two-dimensional space, we get the DOS $g(E_x, E_y)$ and N(T) as

$$g(E_x, E_y) \sim \frac{\sqrt{m}}{\hbar^2 c} \frac{1}{\sqrt{E_x}}$$

$$N(T) \sim \frac{\sqrt{m}}{\hbar^2 c}(k_B T)^{3/2} \tag{44}$$

In Figure 5, we summarize the above results in a pictorial way.

6. Newton's law of cooling

The law of cooling due to Newton states that the rate of loss of heat by a body, due to radiation, is directly proportional to the temperature difference between the body and the
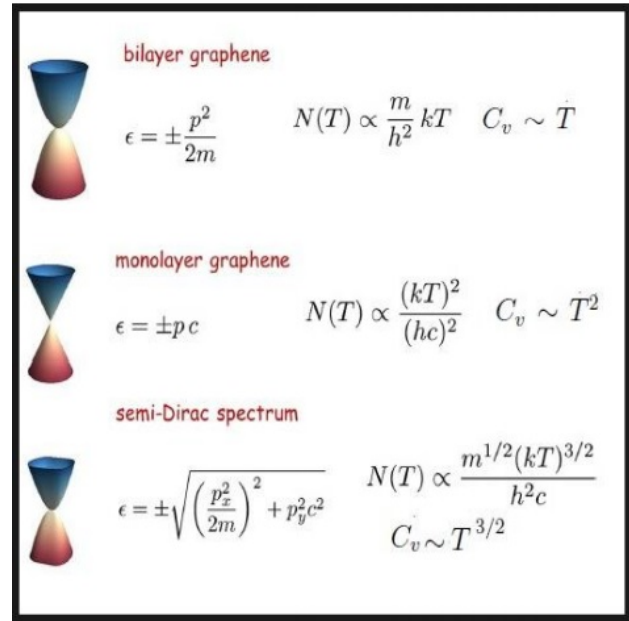
Figure 5: Dispersion spectra and Specific heat of two dimensional systems. Reproduced from reference [35].

surroundings under the assumption that the temperature difference is rather small. It is interesting to point out that Newton's law of cooling however does not take into the consideration the fact that a body can cool by both radiation and convection, it rather takes only radiation (which is indeed a limitation of this law). One can in fact justify this law from Stfean-Boltzmann law in the following way. If T_0 is the surrounding's temperature, then in terms of emissivity e and area A, we can recast Stfan-Boltzmann law as

$$-\frac{dQ}{dt} = Ae\sigma\left(T^{\frac{d}{s}+1} - T_0^{\frac{d}{s}+1}\right) \tag{45}$$

Now assuming $T = T_0 + x$ where x being small temperature, we can rewrite as

$$-\frac{dQ}{dt} = Ae\sigma T_0^{\frac{d}{s}+1}\left[\left(1+\frac{x}{T_0}\right)^{\frac{d}{s}+1}-1\right]$$

$$= Ae\sigma T_0^{\frac{d}{s}}\left(1+\frac{d}{s}\right)(T-T_0) \qquad (46)$$

If m and C_V be the mass and specific heat at constant volume of the material of the black body, then the rate of charge of temperature follows a simple differential equation given by

$$-mC_V\frac{d\theta}{dt} = Ae\sigma T_0^{\frac{d}{s}}\left(1+\frac{d}{s}\right)(T-T_0)$$

$$-\frac{d\theta}{dt} = K_d(T-T_0) \qquad (47)$$

Thus, although Newton's law of cooling is valid for the instantaneous rate of change of the temperature, however, through the equation (47) we can get the complete history of the temperature fall of the body. Since K_d essentially depends on the arbitrary dimension d, the rate of fall of temperature will be different in different spatial dimensions. The rate of fall will be faster in three dimension compared to two and one dimensional space.

7. Conclusions

To conclude, we have discussed the various features of black body radiation emanated by particles with a dispersion relation $\omega \sim k^s$ ($s > 0$) in an arbitrary spatial dimension d. As a result, Stefan-Boltzmann's law also depends on both the spatial dimension d and the power s of the dispersion law.

8. Set of Problems

1. The filament of a light bulb is cylindrical with length $l = 20mm$ and radius $r = 0.05mm$. The filament is maintained at a temperature $T = 5000K$ by an electric current. The filament behaves approximately as a black body, emitting radiation isotropically. At night, you observe the light bulb from a distance $D = 10km$ with the pupil of your eye fully dilated to a radius $\rho = 3mm$.

   (a) What is the total power radiated by the filament?

   (b) How much radiation power enters your eye?

   (c) At what wavelength does the filament radiate the most power?

   (d) How many radiated photons enter your eye every second? Is this signal detectable by a human eye? You can assume that the average wavelength for the radiation is $\lambda = 600nm$. [Ans. (a) 220 W (b) $4.95 \times 10^{12}W$ (c) 580 nm (d) $1.5 \times 10^7 photons/s$; Yes]

2. Cosmic Microwave Background (CMB) is a black body radiation whose temperature is 2.725 ± 0.002 K. Using Wien's displacement law, compute the peak wavelength and frequency of this CMB. Which particular region of electromagnetic radiation does it belong to? Hence, sketch a typical radiation spec-

tra. [Ans.(a) $1.063 \times 10^3 m$, 283 GHz, Radio wave]

3. Stephen Hawking showed that entropy of the non-rotatong uncharged black hole as

$$S = \frac{k_B c^3 A}{4G\hbar}$$

where A is the area of the blackhole given as $4\pi R_S^2$ with $R_S = \frac{2GM}{c^2}$.

(a) Argue that the above formula is dimensionally correct.

(b) Compute the temperature (θ_H) of the black hole.

(c) If the black holes radiate according to Stefan-Boltzmann law, then they will lose mass. Assuming the rate of change of mass is given by

$$c^2 \frac{dM}{dt} = -A\sigma T^4 \,.$$

Find the variation in the mass of blackhole as a function of time. Now, assuming the initial mass $M(0) = 2 \times 10^{11} Kg$, show that the black hole evaporates in a time of $t = 7 \times 10^{11} \, second$, which is nothing but the age of the universe.

(d) If this black hole is exposed to CMB radiation with a temperature θ_B, then the black holes will gain energy through CMB but lose energy through Hawking radiation. In such a situation, find the mass (m_0) in terms of θ_B and other fundamental constants at which the energy exchanges reach equilibrium. Is this equilibrium stable? Explain.[Ans. (i) $\frac{\hbar c^3}{8\pi G k_B M}$. See [9] for more exotic problems on black holes based on dimensional analysis.]

4. An unknown magnetic sample shows a straight line graph with non-zero intercept when $\frac{C}{T^{3/2}}$ is plotted against $T^{3/2}$, where C is the specific heat at low temperature. Is it possible to identify the nature of the magnetic sample? How will the specific heat change when the dimensionality of the system changes to two? [Ans; Ferromagnetic Insulator in three dimensions. $C_{2d} = AT + BT^2$.]

Acknowledgments

References

[1] M. Planck, *Berlin Academy of Sciences*, **X**, 19 (1900).

[2] M. Planck, *Berlin Academy of Sciences*, **XII**, 14 (1900).

[3] M. Planck, *Annalen der Physik*, **14**, 553 (1901).

[4] M. Planck, *Annalen der Physik*, **37**, 642 (1912).

[5] G. S. Ranganath, Black-body Radiation, *Resonance*, **13**, No.2, 115 (2008).

[6] John Crepeau, A BRIEF HISTORY OF THE T^4 RADIATION LAW, Proceedings HT 2009 2009 ASME Summer Heat Transfer Conference July 19-23, 2009, San Francisco, California USA, HT2009-88060

[7] Jonathan M. Marr and Francis P. Wilkin, A better presentation of Planck's radiation law, *Am. J. Phys.*, **80**, 399 (2012).

[8] Ke Xiao, Dimensionless Constants and Blackbody Radiation Laws, *Electronic Journal of Theoretical Physics (EJTP)*, **8**, No. 25, 379 (2011).

[9] Praveen Pathak, Vinay Uppal and Vijay A. Singh, Exploring Black Hole Physics via Dimensional Analysis, *Resonance*, **13**, No. 5, 475 (2008).

[10] A. G. Agnese, M. La Camera and E. Recam, *Black-body laws derived from a minimum knowledge of Physics*, ArXiv:9907008.

[11] D. Jana, *Dimensional Analysis: Modern Perspectives* (Lambert Academic Publishing (LAP), Germany, 2011).

[12] D. Jana, *Phys. Edu.*, **25**, 35 (2008). See also, *Phys. Edu.*, **32**, No. 1, Article No.1, (2016).

[13] J. Dryzek and K. Ruebenbauer, Planck's constant determination from blackbody radiation. *Am. J. Phys.*, **60(3)**, 251 (1992).

[14] I. Bonnet and J. Gabelli J, Probing Planck's law at home, *Eur. J. Phys.*, **31**, 1463 (2010).

[15] Adam Usman, John Dogari, M. Ridwan Enuwa and Isa Sambo, A tutorial on laboratory determination of Planck's constant from the Planck radiation law, Lat. *Am. J. Phys. Educ.*, **3**, 246 (2009).

[16] Francisco J Abellan et al., The Stefan-Boltzmann constant obtained from the I-V curve of a bulb, *Eur. J. Phys.*, **34** 1221 (2013).

[17] Ronald J. Adler, Six easy roads to the Planck scale, *Am. J. Phys.*, **78**, 925 (2010).

[18] T. H. Boyer, *Am. J. Phys.*, **86**, 280 (2018).

[19] W Wien, *Ann. Physik.*, **58**, 622 (1896).

[20] P. Pesic, *Am. J. Phys.*, **75**, 457 (2005).

[21] J Stefan, Sitzungsberichteder Kaiserlichen Akademie der Wissenschaften, Mathematische Naturwissenschaftliche Classe Abteilung, **279**, 391 (1879).

[22] L Boltzmann, *Annalender Physik und Chemi.*, **22**, p.31, 291, (1884).

[23] Francisco J Abellan et al., *Eur. J. Phys.*, **34**, 1221 (2013).

[24] I. Ahmad, S. Khalid, and E. E. Khawaja, Filament temperature of low power incandescent lamps: Stefan-Boltzmann law, *Lat. Am. J. Phys. Educ.*, **4**, 74, (2010).

[25] Vittorio Zanetti, Temperature of incandescent lamps, *Am. J. Phys.*, **53(6)**, 546 (1985).

[26] E. M. Wray, A Simple test of Stefans law, *Phys. Educ.(U.K)*, **10**, 25 (1975).

[27] Marcello Carla, Stefan-Boltzmann law for the tungsten filament of a light bulb:Revisiting the experiment, *Am.J. Phys.*, **81**, 512 (2013).

[28] D. C. Agrawal and V. J. Menon, Lifetime and temperature of incandescent lamps, *Phys. Educ.*, **33**, 55 (1998).

[29] B. S. N. Prasad and R. A. Mascarenhas, Laboratory experiment on the application of Stefan's law to tungsten filament electric lamp, *Am. J. Phys.*, **46**, 420 (1978).

[30] H. S. Leff, Illuminating physics with light bulbs, *The Phys. Teacher*, **28**, 30 (1990).

[31] B. Denardo, Temperature of a lightbulb filament, *The Phys. Teacher*, **40**, 101 (2002).

[32] W. R. BIevin and W. J. Brown, A Precise Measurement of the Stefan-Boltzmann Constant, *Metrologia*. **7**, 15 (1971).

[33] R. F. Rodriguez and L. S. Garcia-Colin, *Eur. J. Phys.*, **10**, 214 (1989).

[34] H Paul et al, The Stefan Boltzmann law: two classical laws give a quantum one, *Phys. Scr.*, **2015**, 014027 (2015).

[35] G. Montambaux, Generalized Stefan-Boltzman Law, *Found. Phys.*, **March 2018**, Page 1 (Springer).

[36] T. H. Boyer, *Eur. J. Phys.*, **37**, 065102 (2016). See also, T. H. Boyer, *Found. Phys.*, **40** 1102 (2010). T. H. Boyer, *Phys. Rev. D*, **81**, 105024 (2010). T. H. Boyer, *Am. J. Phys.*, **79**, 644 (2011). T. H. Boyer, *Found. Phys.*, **42**, 595 (2012). T. H. Boyer, *Eur. J. Phys.*, **38**, 045101 (2017).

[37] Tatiana R. Cardoso and Antonio S. de Castro, *The Blackbody Radiation in D-Dimensional Universes*, arXiv:quant-ph/0510002v1.

[38] It can be established theoretically that the equation connecting the frequency of maximum energy intensity in units of $Joules/m^3/Hz$ is:$f_{max} = 5.88 \times 10^{10} THz/K$. While the most common stated law is in terms of the wavelength at $Joules/m^3/m$: $\lambda_{max} = \frac{2.89 \times 10^{-3}}{T}$ mK.The interesting point to notice here is that these formulae do not give the same result (as is easily verified, since $f_{max}\lambda_{max} = 1.7 \times 10^8 m/sec$, not the speed of light. The reason is that the two measures, per unit interval of frequency and per unit interval of wavelength, are different. When it is claimed that sun light is most intense

in the yellow, one has to specify which is being used (actually it would be in wavelength rather than the frequency). In fact frequency indicates near the infrared.

[39] P. T. Landsberg and A. De Vos, The Stefan-Boltzmann constant in n-dimensional space, *J. Phys. A: Math. Gen.,* **22** 1073 (1989).

Why no radiation occurs in the case of a uniformly accelerated charge

Ashok K. Singal

Astronomy and Astrophysics Division, Physical Research Laboratory
Navrangpura, Ahmedabad 380 009, India.

ashokkumar.singal@gmail.com

Submitted on 23-09-2018

Abstract

We show that in the case of a uniformly accelerated charge, in its instantaneous rest frame, there is only a radial electric field as the acceleration fields strangely get cancelled *at all distances* by a transverse term of the velocity fields. Consequently, no electromagnetic radiation will be detected by any observer from a uniformly accelerated charge, even in the far-off zone. This is in contradiction with Larmor's formula, according to which a uniformly accelerated charge would radiate power at a constant rate, which is proportional to the square of the acceleration. On the other hand, the absence of radiation from such a charge is in concurrence with the strong principle of equivalence, where a uniformly accelerated charge is equivalent to a charge permanently stationary in a gravitational field, and such a completely time-static system could not be radiating power at all.

1 Introduction

According to Larmor's formula, an accelerated charge radiates electromagnetic power at a rate proportional to the square of its acceleration [1, 2, 3, 4]

$$\mathcal{P} = \frac{2e^2\dot{\mathbf{v}}^2}{3c^3} \,. \tag{1}$$

However, the net rate of momentum loss to radiation by such a charge is nil

$$\dot{\mathbf{p}} = 0 \,, \tag{2}$$

because of the azimuthal symmetry ($\propto \sin^2\phi$) of the radiation pattern, at least in the case of a non-relativistic motion [2, 3, 4], and consequently the formula leads to a violation of the energy-momentum conservation law [5]. Moreover, from the strong principle of equivalence, a uniformly accelerated charge is equivalent to a charge permanently stationary in a gravitational field [6] and in such a completely time-static system, there cannot be radiation of power at any instant, let alone a continuous radiation for an indefinite time interval.

From a careful scrutiny of the electromagnetic fields of a uniformly accelerated charge, we shall show that there is no electromagnetic radiation anywhere, not even in the far-off regions. As we will explicitly demonstrate, this happens because the acceleration fields get cancelled neatly by a transverse component of velocity fields, at all distances. As a result, there is no Poynting flux with a term proportional to the square of acceleration, usually called the radiated power, implying thereby that no electromagnetic radiation takes place from a uniformly accelerated charge.

2 Electromagnetic fields of a uniformly accelerated charge − no evidence of radiation anywhere

A uniformly accelerated motion usually implies a motion with a constant proper acceleration, say, $\mathbf{g}$. We may assume it to be a one-dimensional motion, as we can always transform to another inertial frame so as to make the component of the velocity vector in a direction perpendicular to the acceleration vector zero.

We shall now explicitly demonstrate that in the instantaneous rest frame of a charge with a constant proper acceleration, there is a complete cancellation of acceleration fields by a transverse term in the time-retarded velocity fields *at all distances*.

Electromagnetic fields of a charge e, moving in one dimension with a proper ac-

celeration $\mathbf{g}$ $(= \gamma^3 \dot{\mathbf{v}})$, can be written for any given time t as [2, 3, 4, 7]

$$\begin{aligned}
\mathbf{E} &= \left[\frac{e(\mathbf{n} - \mathbf{v}/c)}{\gamma^2 r^2 (1 - \mathbf{n} \cdot \mathbf{v}/c)^3} \right. \\
&\quad \left. + \frac{e\,\mathbf{n} \times (\mathbf{n} \times \mathbf{g})}{\gamma^3 r c^2 \,(1 - \mathbf{n} \cdot \mathbf{v}/c)^3} \right]_{t'} \\
\mathbf{B} &= \mathbf{n} \times \mathbf{E}, \tag{3}
\end{aligned}$$

where the subscript t' indicates that quantities within the square bracket are to be evaluated at the corresponding retarded time $t' = t - r/c$.

Now, for a one-dimensional motion with a constant proper acceleration $\mathbf{g}$, the velocity $\mathbf{v}$ at the retarded time $t - r/c$ is obtained from its *present* value $\mathbf{v}_o$ at time t (with γ, γ_0 being the corresponding Lorentz factors) as

$$\gamma \mathbf{v} = \gamma_0 \mathbf{v}_0 - \mathbf{g} r/c. \tag{4}$$

Therefore, in the instantaneous rest-frame ($\mathbf{v}_0 = 0$), the proper acceleration and the *retarded value* of the velocity are related by $\gamma \mathbf{v} = -\mathbf{g} r/c$. Basically this happens because for larger r, we need to go further back in time to get the time-retarded value of velocity, which, in the case of a uniform acceleration, is directly proportional to the time interval r/c. Substituting for $\mathbf{g}$ in Eq. (3), and after a rearrangement of terms, we get the electric field in the instantaneous rest-frame as

$$\mathbf{E} = \left[\frac{e(\mathbf{n} - \mathbf{v}/c - \mathbf{n} \times \{\mathbf{n} \times \mathbf{v}/c\})}{\gamma^2 r^2 (1 - \mathbf{n} \cdot \mathbf{v}/c)^3} \right]_{t'}. \tag{5}$$

Using the vector identity $\mathbf{n} \times (\mathbf{n} \times \mathbf{v}) = \mathbf{n}(\mathbf{n}.\mathbf{v}) - \mathbf{v}$, we get the expression for the

electric field in the instantaneous rest-frame of a uniformly accelerated charge as

$$\mathbf{E} = \left[\frac{e\mathbf{n}}{\gamma^2 r^2 (1 - \mathbf{n} \cdot \mathbf{v}/c)^2} \right]_{t'}, \qquad (6)$$

where there is only a radial electric field with respect to the charge position at the retarded time, with the transverse acceleration fields in Eq. (3) having got cancelled by transverse component of velocity fields, for all r. There is thus neither any magnetic field nor Poynting flux *anywhere* and therefore no observer would detect any radiation at whatever distance, in the instantaneous rest frame.

This in turn is in agreement with the strong principle of equivalence where a charge permanently stationary in a gravitational field, and thereby with no whatsoever temporal variations, and which is equivalent to a charge having a constant proper acceleration [6], cannot be continually radiating [8, 9].

At any other time, when $\mathbf{v}_o \neq 0$, in addition to the radial term in Eq. (6), we also have a transverse term for the electric field

$$\begin{aligned} \mathbf{E} \;=\; \Big[& \frac{e\mathbf{n}}{\gamma^2 r^2 (1 - \mathbf{n} \cdot \mathbf{v}/c)^2} \\ & + \frac{e\mathbf{n} \times \{\mathbf{n} \times \gamma_0 \mathbf{v}_0/c\}}{\gamma^3 r^2 (1 - \mathbf{n} \cdot \mathbf{v}/c)^3} \Big]_{t'}. \end{aligned} \qquad (7)$$

Now the transverse terms, proportional to the present velocity $\gamma_0 \mathbf{v}_0$, fall rapidly with distance ($\propto 1/r^2$); the Doppler beaming factor $\delta^3 = 1/\gamma^3 (1 - \mathbf{n} \cdot \mathbf{v}/c)^3$ merely redistributing the field strength in solid angle without affecting the net Poynting flux at any r. From Poynting vector, $\mathbf{S} = c(\mathbf{E} \times$

$\mathbf{B})/4\pi$, Eq. (7) yields for the Poynting flux through a spherical surface, Σ of radius r [9]

$$\mathcal{S} = \int_\Sigma \mathrm{d}\Sigma \, (\mathbf{n} \cdot \mathbf{S}) = \frac{2e^2}{3cr^2} (\gamma_0 v_0)^2. \qquad (8)$$

We see that the Poynting flux falls rapidly with distance ($\mathcal{S} \to 0$ as $r \to \infty$). Here we find no term independent of r and proportional to $\dot{\mathbf{v}}^2$, that is usually defined as the radiated power, implying thereby, no radiation from a uniformly accelerated charge.

To fully comprehend its physical implications, we replace the uniformly accelerated charge at its position at the retarded time t', by a charge moving with a uniform velocity v_0 (equal to the "present velocity" of the accelerated charge). The electric field for such a charge can be written as

$$\begin{aligned} \mathbf{E} \;=\;& \left[\frac{e(\mathbf{n} - \mathbf{v}_0/c)}{\gamma_0^2 r^2 (1 - \mathbf{n} \cdot \mathbf{v}_0/c)^3} \right]_{t'} \\ =\;& \Big[\frac{e\mathbf{n}}{\gamma_0^2 r^2 (1 - \mathbf{n} \cdot \mathbf{v}_0/c)^2} \\ & + \frac{e\mathbf{n} \times \{\mathbf{n} \times \gamma_0 \mathbf{v}_0/c\}}{\gamma_0^3 r^2 (1 - \mathbf{n} \cdot \mathbf{v}_0/c)^3} \Big]_{t'}, \end{aligned} \qquad (9)$$

where we have used the vector identity $\mathbf{v}_0 = \mathbf{n}(\mathbf{n}.\mathbf{v}_0) - \mathbf{n} \times (\mathbf{n} \times \mathbf{v}_0)$.

Now, in this case too we get the same Poynting flux (Eqs.(8)) through a spherical surface around the retarded position of the charge. This is true for any r. As for a charge moving with a uniform velocity, a finite Poynting flux certainly does not imply power being radiated away from the charge, it is merely due to the movement of the charge along with its self-fields, with a ve-

locity v_0 with respect to the retarded position upon which the spherical surface is centred. Same is the case of a uniformly accelerated charge which has a "present" velocity v_0 with respect to its retarded position and therefore it does not represent any power being radiated away from the charge.

3   What is amiss in Larmor's radiation formula?

A pertinent question that could arise here is: If a uniformly accelerated charge does not radiate, which contradicts Larmor's formula, does it mean that Larmor's formula is invalid? How could this issue be resolved?

Actually, in the text-book derivation of Larmor's formula (Eqs.(1)), Poynting's theorem is improperly applied to equate the radiated power at time t to the rate of loss of the mechanical energy $(\mathcal{E}_{me})$ of the charge at a retarded time $t' = t - r/c$

$$\left[\frac{d\mathcal{E}_{me}}{dt}\right]_{t'} = -\left(\int_\Sigma d\Sigma\,(\mathbf{n}\cdot\mathbf{S})\right)_t. \quad (10)$$

However, in Poynting's theorem *all quantities* are supposed to be calculated for the *same instant of time* [2, 3, 4], say, t and one cannot directly calculate the rate of loss of the mechanical energy $(\mathcal{E}_{me})$ of the charge at a retarded time $t' = t - r/c$ from the radiated power at time t.

That Eq. (10) could lead to wrong conclusions can be seen by applying it to the case of an accelerated charge that is instantly stationary at t'. The charge has no velocity at that instant and hence no kinetic en-

ergy, therefore the left hand side can only be zero, while the right hand side yields a finite result for the Poynting flux (proportional to square of the acceleration of the charge, with no dependence on velocity). Therefore the derivation of Larmor's formula (Eqs.(1)) employing Eqs.(10) may not be a legitimate one and it is this oversight which could mostly be responsible for the confusion in this century-old problem.

It is important to note that in the case of a periodic motion of period T, there is no difference in the radiated power integrated or averaged between t to $t + T$ and t' to $t' + T$, therefore Eq.(10), and thereby Larmor's formula, does yield a correct average power loss by the charge for a periodic case. Further, for a periodic motion, e.g., a harmonically oscillating charge in a radio antenna, it is easily verified that $< \dot{\mathbf{v}}^2 > = < -\ddot{\mathbf{v}}\cdot\mathbf{v} >$ [10], therefore Larmor's formula (Eqs.(1) yields the same time-averaged radiative power as from the formula derived from the famous Abraham-Lorentz radiation reaction formula [11, 12, 13, 14, 15], where one gets instantaneous power loss of the charge (in a non-relativistic motion) as [10]

$$\mathcal{P} = -\frac{2e^2}{3c^3}\ddot{\mathbf{v}}\cdot\mathbf{v}. \quad (11)$$

However, in a non-periodic motion, as in the case of a uniform acceleration, Larmor's formula does lead to wrong conclusions. Once this fact is realized, much of the doubt or confusion in this long-drawn-out controversy disappears.

4 Electromagnetic fields in terms of the "real-time" motion of the charge

It is possible to solve the expression for electromagnetic fields of a uniform accelerated charge, not necessarily in terms of motion of the charge at retarded time as in Eqs. (7), instead wholly in terms of the "real-time" motion of the charge [16]. Now, without any loss of generality, we can choose the origin of the coordinate system so that $\alpha = c^2/g$, then the position and velocity of the charge at a time t are given by $z_c = (\alpha^2 + c^2t^2)^{1/2}$ and $v = c^2t/z_c$. Due to the cylindrical symmetry of the system, it is convenient to employ cylindrical coordinates (ρ, ϕ, z). The electromagnetic fields at time t can then be written as [17]

$$
\begin{aligned}
E_\rho &= 8e\alpha^2\rho z/\xi^3 \\
E_z &= -4e\alpha^2(z_c^2 - z^2 + \rho^2)/\xi^3 \\
B_\phi &= 8e\alpha^2\rho ct/\xi^3 \,,
\end{aligned}
\tag{12}
$$

where $\xi = [(z_c^2 - z^2 - \rho^2)^2 + 4\alpha^2\rho^2]^{1/2}$. The remaining field components are zero. Our discussion pertains to the region $z + ct > 0$ because fields only within this region could have any causal relation with the retarded positions of the charge [17].

The charge happens to be at the same location at times t and $-t$, i.e., $z_c(t) = z_c(-t)$. Then from Eq. (12) it can be seen that the electric field **E** (with components E_ρ, E_z) is an even function of time, i.e., at any given location (ρ, ϕ, z), $\mathbf{E}(t) = \mathbf{E}(-t)$. On the other hand, the magnetic field **B** (with a component B_ϕ) is an odd function of time, i.e., $\mathbf{B}(t) = -\mathbf{B}(-t)$, with $\mathbf{B} = 0$ at $t = 0$. Thus there is no Poynting vector, ($\propto \mathbf{E} \times \mathbf{B}$), seen anywhere at $t = 0$. Further, at any given location, the Poynting vector at time t is equal and opposite to its value at $-t$.

Now at $t = 0$, any radiation emitted in past at any time (say, $t = -t_1 < 0$) should be visible as a Poynting flux passing through a spherical surface of radius $r_1 = ct_1$ around the corresponding retarded position of the charge. But the fact that the Poynting vector is seen *nowhere* at $t = 0$, implies absence of any radiation emanating from charge at all $t = -t_1 < 0$. Moreover, corresponding to any event on the charge trajectory even at $t > 0$, we can always find an inertial frame which is the instantaneous rest frame of the charge, and in that frame we can thus conclude that no radiation has taken place from the charge at any past event which is in conformity with the assertion that no radiation *ever* takes place from a uniformly accelerated charge. Incidentally, Pauli [18], exploiting Born's solutions [16], drew attention to the fact that in the instantaneous rest-frame of a uniformly accelerated charge, $\mathbf{B} = 0$ throughout, and from that he inferred that there might be no radiation for such a motion.

It has been said in literature that the radiation emitted by a uniformly accelerated (or decelerated) charge goes into regions of space-time inaccessible to a co-accelerating observer [19]. For instance, there are discontinuous δ-fields present in the $z = 0$ plane

at time $t = 0$, and it is the conjecture that all the radiation emitted by the charge during its uniform acceleration until $t = 0$ has gone into these δ-fields [20]. However, these δ-fields could have no causal relation with the charge during this period, instead the δ-fields have causal relation with the charge at time $t = -\infty$ and actually represent the original velocity fields of the charge prior to the onset of acceleration at that time [9]. The energy in the δ-fields could, at most, be representing the energy loss by the charge due to a *rate of change of acceleration* (Eq. (11)), when the acceleration rose from initial zero value to attain a final constant value, $\mathbf{g}$, at $t = -\infty$. It has been explicitly demonstrated [9] that there is no Poynting flow across the $z = 0$ plane at $t > 0$ and that the field energy in regions of space-time inaccessible to a co-accelerating observer actually appears at the cost of a steady reduction of energy in δ-fields.

Now, let Σ be a fixed finite spherical surface surrounding the charge at t_1. The same surface Σ surrounds the charge at $-t_1$ as well, because $z_c(t_1) = z_c(-t_1)$. The Poynting vector at any point on the surface Σ at time t_1 is exactly equal but opposite to its value at time $-t_1$. Therefore Poynting flux through Σ

$$\mathcal{S} = \int_{\Sigma} d\Sigma \, (\mathbf{n} \cdot \mathbf{S}) \qquad (13)$$

at time t_1 is equal and opposite to that at $-t_1$. Thus while there may be an *outflow* of Poynting flux through surface Σ at time t_1, but there is an equal *inflow* of Poynting flux

through surface Σ at time $-t_1$. This assertion is true for any spherical surface of any radius around the charge, and is therefore not consistent with there being always an outflow of radiation from a surface surrounding an accelerated (or for that matter even a decelerated) charge, as given by standard radiation formulas.

The electromagnetic field energy in a volume $\mathcal{V}$ is given by the volume integral

$$\frac{1}{8\pi} \int_{\mathcal{V}} dV \, (E^2 + B^2). \qquad (14)$$

The field energy density, $(E^2 + B^2)/8\pi$, being equal at times t_1 and $-t_1$, its volume integral over *any chosen* $\mathcal{V}$, even in some far-off zone, is also equal at times t_1 and $-t_1$. Actually, from detailed calculations it has been shown [9] that the total electromagnetic field energy in the case of a uniformly accelerated charge, including the contribution of the acceleration fields as well, at any instant is very much the same as that of a charge moving uniformly with a velocity equal to the instantaneous "present" velocity of the accelerated charge. Thus as the charge velocity increases (during the acceleration phase), its net field energy would increase accordingly and the outflow of Poynting flux represents the increasing field energy. On the other hand, as the charge slows down (during the deceleration phase), its net field energy accordingly decreases and the inflow of Poynting flux represents the decreasing field energy in the space throughout.

This deduction is reinforced by the fact that the field energy of the charge is the

same at t_1 and $-t_1$ since the charge at those two instants is moving with equal speeds (even if in opposite directions). However, there is no trace of any additional energy in electromagnetic fields corresponding to the energy radiated in the intervening period.

One can also compute the electromagnetic field momentum contained within a volume $\mathcal{V}$ from

$$\frac{1}{4\pi c} \int_{\mathcal{V}} \mathrm{d}V \, (\mathbf{E} \times \mathbf{B}). \qquad (15)$$

Since $\mathbf{B} = \mathbf{0}$ at $t = 0$ (Eq. (12)), there is no momentum in the electromagnetic fields anywhere, in the instantaneous rest frame.

Further, for $t \neq 0$, from Eq. (15) in conjunction with Eq. (12), the electromagnetic field momentum within *any chosen* $\mathcal{V}$, even in some far-off zone, is not only equal but in opposite directions at times t_1 and $-t_1$. Now, this fits the expectation that since the charge occupies the same location but has equal and opposite velocities at t_1 and $-t_1$, any given volume element should contribute to the self-fields equal and opposite field momentum, proportional to the "present" velocity, at t_1 or $-t_1$. From the cylindrical symmetry of electromagnetic fields (Eq. (12)), it is easily seen that the net electromagnetic field momentum, integrated over all space, is directly proportional to the instantaneous velocity $\mathbf{v}$ of the charge. However, there is no trace of any additional momentum being carried away by radiation fields which would even otherwise have different angular distributions, due to Doppler beaming along opposite directions of velocities, at t_1 and $-t_1$.

5 Conclusions

We showed that contrary to the predictions of Larmor's/Liénard's radiation formula, no observer anywhere would detect any radiation from a uniformly accelerated charge, in agreement with the absence of electromagnetic radiation from such an accelerated charge. This conclusion is also in accordance with the strong principle of equivalence.

References

[1] J. Larmor, Phil. Mag. 44 (1897) 503

[2] J. D. Jackson, Classical electrodynamics, 2nd ed. (Wiley, New York, 1975)

[3] W. K. H. Panofsky and M. Phillips, Classical electricity and magnetism, 2nd ed. (Addison-Wesley, Massachusetts, 1962)

[4] D. J. Griffiths, Introduction to electrodynamics, 3rd ed. (Prentice, New Jersey, 1999)

[5] A. K. Singal, J. Phys. Commun. 2 (2018) 031002

[6] C. W. Misner, K. S. Thorne and J. A. Wheeler, Gravitation (Freeman: San Fransisco, 1973)

[7] A. K. Singal, Am. J. Phys. 79 (2011) 1036-1041

[8] A. K. Singal, Gen. Rel. Grav. 27 (1995) 953-967

[9] A. K. Singal, Gen. Rel. Grav. 29) (1997) 1371-1390

[10] A. K. Singal, Eur. J. Phys. 37 (2016) 045210

[11] Abraham M., Ann. Phys. 14 (1904) 236

[12] M. Abraham, Theorie der elektrizitat, Vol II: Elektromagnetische theorie der strahlung (Teubner, Leipzig, 1905)

[13] H. A. Lorentz, Encykl. Mathe. Wiss. 2 (1904) 145-280

[14] H. A. Lorentz, The theory of electron (Teubner, Leipzig, 1909); 2nd ed. (Dover, New York, 1952)

[15] A. K. Singal, Am. J. Phys. 85 (2017) 202-206

[16] M. Born, Ann. Physik 30 (1909) 1-56

[17] T. Fulton and F. Rohrlich, Ann. Phys. 9 (1960) 499-517

[18] W. Pauli Relativitätstheorie in Encyklopadie der Matematischen Wissenschaften, V 19 (Teubner, Leipzig, 1921) Translated as Theory of relativity (Pergamon, London, 1958)

[19] C. de Almeida and A. Saa, Am. J. Phys. 74 (2006) 154-158

[20] D. G. Boulware, Ann. Phys. 124 (1980) 169-188

Alpha Spectrum of ^{212}Bi Source Prepared using Electrolysis of Non-Enriched ThNO$_3$ Salt

Swapna Gora[1], B.P. Jithin[1], V.V.V. Satyanarayana[2], O.S.K.S Sastri[1] and B.P Ajith[2]

[1]Department of Physics, Central University of Himachal, HP 176215, India.
sastri.osks@gmail.com

[2]Inter University Accelerator Centre, New Delhi, India.
ajith@iuac.res.in

Submitted on 03-07-2018

Abstract

We present various aspects involved in performing alpha spectroscopy experiments using non-enriched *ThNO$_3$* salt. The experimental design is improved in a cyclic fashion to bring forth the importance of thin film preparation of the radioactive source, and creating vacuum in reducing the energy losses due to self-absorption and air scattering respectively. Thin film preparation using electrolysis of *ThNO$_3$* aqueous solution has been optimized for current and time to selectively deposit ^{212}Bi. The obtained spectrum had large peaks at 6093 keV and 8753 keV with resolutions of 2.10% and 2.90% and relative percentage errors of 0.59% and 0.35% respectively. These peaks had intensity ratios of 33.2% : 66.8% matching with existing values in Nuclear Data Tables. Then the concentration (ratio of *ThNO$_3$*:water) has been increased to obtain reasonably large counts within 4 hours so that data can be utilised to obtain half life of ^{212}Bi. The best obtained half life of Bismuth from the counts saved after every 20 minutes has been determined to be 62.77 ± 0.79 minutes which is close to the expected value of 60.55 ± 0.30 minutes.

1 Introduction

UGC guidelines [1] 2015 for B.Sc. Hons in Physics has included a course on Radiation Safety, with 30 lectures, and insists on a set of experiments to be performed using GM counters for radiation detection, Spark counter for alpha detection and Gas Light mantle (source of Thorium) for obtaining gamma spectrum. While this course is one of the skill enhancement courses, the discipline specific elective paper on Nuclear and Particle Physics is loaded with 5 credits and only a Tutorial of 1 credit with no lab work.

There are two major difficulties for proposing a nuclear physics lab at both the UG and PG level: The high cost involved in procuring nuclear instrumentation, and the need for radiation safety.

Realising the need for dissemination of knowledge in experimental nuclear physics and the need to create awareness regarding radiation at the UG/PG level in various colleges, Dr.Ajith has taken initiative under the outreach programme of Inter University Accelerator Centre (IUAC), and along with Er. Satyanarayana, developed an alpha spectrometer [2] with associated software in python, all of which are made as open source.

CSpark Research (India) has adopted their basic hardware design comprising of a pre-amplifier and shaping amplifier and re-designed it with enhanced detector and vacuum solution along with a 1K MCA and a user friendly featured software CN-Spec and made it available in the market at very low cost of less than Rs.50,000/-.

Our PER group at Central University of Himachal Pradesh is working on developing a Nuclear Physics lab based on good practices found through research such as (a) establishing learning goals (b) designing activities, simulations and experiments and accordingly revise the curriculum to achieve the desired learning goals and finally (c) create appropriate rubrics to provide precise assessment.

To realise these objectives, we need to address the disadvantages pertaining to cost and safety. In this paper, we are focusing on using CSpark Research's low cost alpha spectrometer **('AlphaSpec-1K')** [3] to perform experiments with non-enriched $Th(NO_3)$ salt which is available from suppliers of chemicals at a reasonable cost of about Rs.5000/- for 100gm.

In the presentation of this paper, we have chosen to follow closely the advanced lab learning goals suggested by University of Colorado, Boulder in [4]. The goals are classified into the following four categories:

1. Modeling (Physical system, measurement apparatus, predicting outcomes and using statistical analysis for comparison)

2. Design (Apparatus, experiments, and troubleshooting)

3. Communication (Argumentation/ thorough analysis and discussion, oral and poster presentation, writing papers etc)

4. Technical lab skills (Basic test and measurement, computer interfacing, computer aided analysis)

The actual listing is available at [4].

In this paper, we shall be focussing on incorporating learning goals about modelling lab experiments based on the experiment involving alpha spectrum of ^{212}Bi. We shall restrict our scope to suit the learners at the UG level.

2   Modeling

In this experiment, designing lab specific learning goals based on modeling framework involves

1. understanding the source, its preparation and characteristics

2. interaction medium, which consists creating a vacuum within the source-detector housing assembly using a rotary vacuum pump

3. measurement process, which has the detection electronics hardware followed by the data acquisition software along with its various features

2.1   Modeling the Source

The source is a non-enriched radioactive sample composed of thorium nitrate $(Th(NO_3).5H_2O)$ in powder form which has ^{232}Th and its various daughter products available via alpha and beta emission. Especially, we are focussing on studying:

1. The α spectrum of ^{212}Bi, one of the final daughters in the series, which results from the process of preparation of thin film source required for reducing the alpha energy losses due to self-absorption.

2. The half-life of ^{212}Bi

The learners' goals are to (i) model the radioactive decay of alpha theoretically and (ii) obtain the quantitative predictions of

observable phenomenon, in this case, the alpha energies that are emitted by ^{212}Bi and its half-life.

Typically, modeling the alpha decay should have been done using Gamow's theory as presented in various books [[6]-[10]]and notes [[11]-[14]]. Here, the focus being ^{212}Bi, which is an odd-odd nuclei, undergoing both α and β decays with significant branching ratios, it is difficult for existing theoretical models as well as phenomenological models such as those using Viola-Seaborg formula [13] to predict its half-life accurately. So, for the sake of making predictions, we resort to already existing experimental data as a basis.

The expected alpha energies of the radioactive decay chain of Thorium-232 are obtained from ENSDF website [12]. These are compiled in Table.1 and labelled from A-G. An alpha-energy is considered only if it has an intensity of atleast 1% or above.

Now, looking specifically at ^{212}Bi, we observe that it has an α-branch with 35.94% and a β-branch with 64.06%. Interestingly, this is the only nuclei among all those appearing in the four naturally occuring radioactive series to be having such a significant branching ratio. Its α-decay proceeds majorly to two closely lying levels in the daughter nucleus ^{208}Tl, with 69.91% and 27.12% towards 6050.78 keV and 6098.88 keV α-energies respectively. If the spectrometer has resolution poorer than 50 keV, it would not be possible to resolve these two peaks and one would obtain a single peak

at the weighted average of the two given by 6061.71keV. Its β decay daughter ^{212}Po has a 100% α-decay route with an extremely short half-life of only 299 ns and hence gives rise to a large peak at 8785 keV. In fact, once again, this is the minimum half-life and the maximum energy for any nuclei appearing in all the naturally occuring radioactive series.

The expected half-life for ^{212}Bi taken from Nuclear Wallet Cards [15] is 60.55 ± 0.30 mins. This could be verified from either of the two branches of ^{212}Bi, as the daughter from its β-decay has negligible half-life.

Finally, students should be made aware of safety issues to be followed while handling the radioactive source. Even though it is a non-enriched source, one should not touch the powder with bare hands, and must take care to never ingest any.

2.2   Modeling of Physical System

'AlphaSpec-1K' alpha spectrometer setup (shown in Figure 1) contains the physical system (source-detector housing assembly along with vacuum pump) and the measurement apparatus (detector electronics hardware along with data acquisition via the USB port of a computer, and its associated software 'CNSpec'.

The physical system in the context is the interacting medium. This leads to another learning goal from the lab point of view. That is, students should gain appreciation with regards to the interacting medium by considering the following points:

1. The detector which is also sensitive to light photons needs to be housed inside a chamber, so that only alphas register their energy inside its active volume.

2. Since alpha particles lose energy due to scattering as they pass through air , we need the source also to be placed in an air tight chamber so that vacuum can be created.

Keeping these points in view, the physical system is designed (see Figure-1) to have an air-tight stainless steel chamber(1) for housing the source and detector. The inner dimensions of the chamber allow for variation of source-detector distance upto 25 mm.

In order to create the required vacuum, a 1/5 BHP rotary vane pump (2) in Figure-1, fitted with a pressure gauge (3) and two valves (A and B) are utilised. While closing the vent valve (A) cuts off the atmosphere from the chamber, the series valve (B) connects the vacuum pump to the chamber to evcuate it down to 1 mbar.

2.3   Modeling of Measurement Apparatus

The next important learning goal is to model the measurement process so that it does not merely remain a black box for the students, and that instead they understand the principles of operation, key model parameters, and limitations on the ideal functioning of the apparatus [4]. The detailed modeling of

Table 1: The radioactive decay chain of ^{232}Th with alpha energies and their respective intensities are complied from ENSDF [12] and labelled from A to G. Only those alphas which have more than 1% intensity are considered. Beta emissions are also shown, but only for the sake of clarity and completeness.

Radioactive Decay Chain of Thorium-232					
Parent Nuclei	Decay Mode	Half Life (a=year)	Energy Released (keV)	Intensity of α-decay branch(%)	Daughter Nuclei
^{232}Th	α	1.405×10^{10} a	3974.2 (A1) 4012.3 (A2)	21.7 78.2	^{228}Ra
^{228}Ra	β⁻	5.75 a	-	-	^{228}Ac
^{228}Ac	β⁻	6.25 h	-	-	^{228}Th
^{228}Th	α	1.9116 a	5340.36 (B1) 5423.15 (B2)	26 73.4	^{224}Ra
^{224}Ra	α	3.6319 d	5448.6 (C1) 5685.37 (C2)	5.06 94.92	^{220}Rn
^{220}Rn	α	55.6 s	6288.08 (D)	99.886	^{216}Po
^{216}Po	α	0.145 s	6778.3 (E)	99.99	^{212}Pb
^{212}Pb	β⁻	10.64 h	-	-	^{212}Bi
^{212}Bi	β⁻ 64.06% α 35.94%	60.55 min	- 6050.78 (F1) 6089.88 (F2)	- 69.91 27.12	^{212}Po ^{208}Tl
^{212}Po	α	299 ns	8784.86 (G)	100	^{208}Pb

the apparatus is discussed in a seprate paper by us [7] to keep this paper from becoming lengthy and also to retain focus on experimentation. Here, we only give a very brief description of the hardware and software specifications.

The Silicon PN junction detector is reverse biased with 9 Volts, and electronic circuits of Pre-amplifier, Shaping amplifier, Peak detector and ADC followed by 1K MCA are integrated at the top part(Figure 1:1(T)) of the chamber to avoid signal losses. The output of the 1K MCA is acquired via USB and is displayed by **'CNSpec'** software provided freely along with the spectrometer.

Hardware Specifications: The design of the electronics is such that the detection system is capable of measuring alpha energies upto 10 MeV with a resolution of 80 KeV for 5.485 MeV energy. The various stages of signal processing electronics are shown as an inset in Figure 1.

At the lower end of the spectrum, spurious events are recorded due to the noise fluctuations in the absence of a signal. In order to reject this, the first 100 channels are not considered while acquiring spectra. **Software Features:** The instrument is factory calibrated using ^{241}Am which is a mono-energetic alpha source. For our instrument, the peak energy of 5485 keV was recorded to be at a centroid value of 495.6 channel. Using this, we can apply a single point calibration. For e.g., the threshold energy corresponding to channel no. 100 using this calibration would be around 800 keV.

The following analytical features are included in the software :

- Curve fitting against standard gaussian function for obtaining the centroid of the peaks. This includes an optional low-energy tail which follows a Lorentzian distribution.

- Summation of counts in a chosen interval to estimate total events from a source which may be spread across a range of adjacent channels due to various reasons such as scattering, noise etc.

- Multi-point calibration with several known peak values.

3   Experimental Design

The design aspect involves varying a particular input parameter, while controlling the rest of the parameters to study the impact on the output obtained. The various aspects involved in the design of the experiment being performed will be based on our understanding of the interactions present. Since, the detection system is already fine tuned by the manufacturer to obtain well resolved spectra, we need to focus only on understanding the source characteristics and interaction of emitted alphas with the environment before reaching the detector.

Typically the radioactive sources that are bought from manufacturer or those obtained from any agencies such as DAE or BARC, would be packaged in the form of a disc of small size smeared with a small
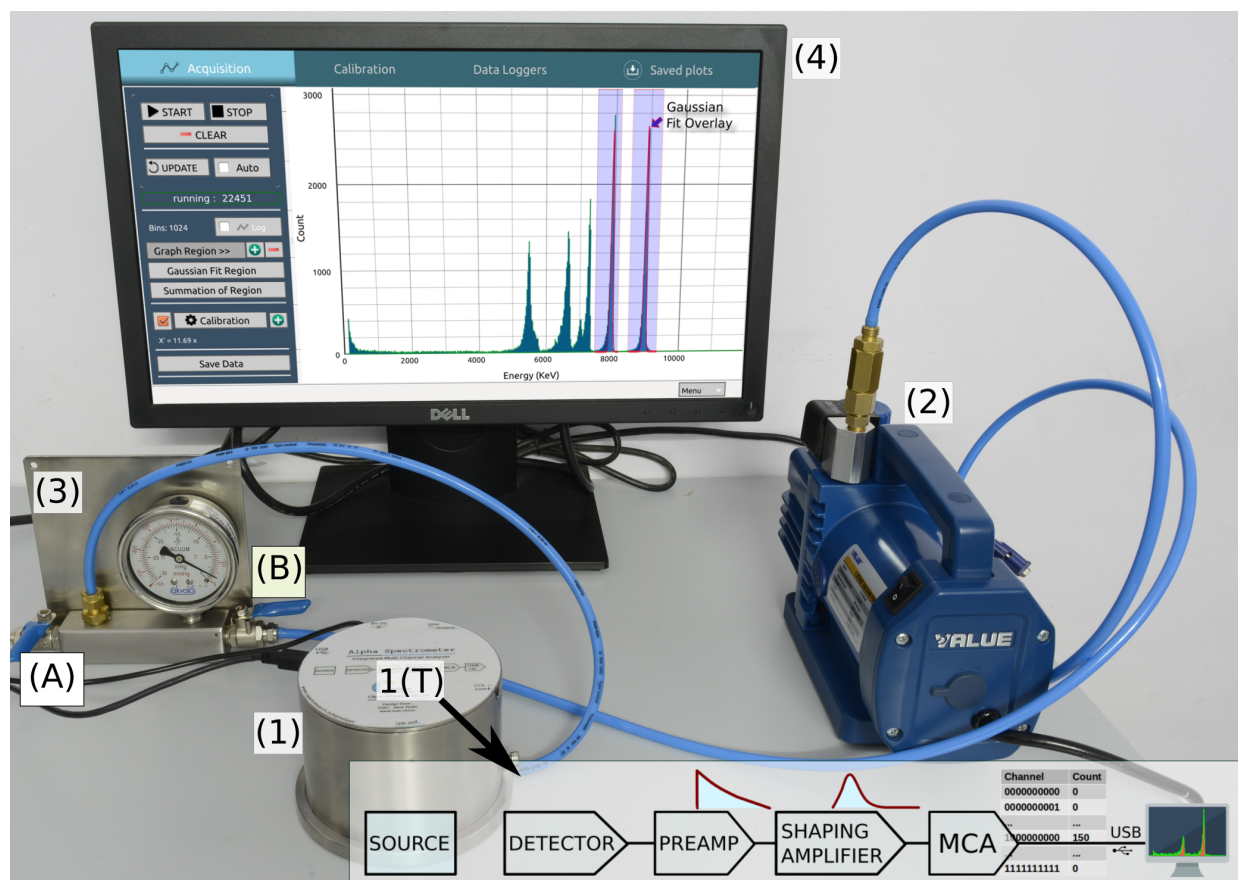
Figure 1: Complete experimental setup for Alpha Spectrometer Alpha-Spec 1K. (1) Chamber for housing source and detector; (1(T)) Detector electronics; Inset shows flow diagram with various stages of signal processing; (2) Rotary Vane pump for creating vacuum; (3) Two way valve with pressure gauge; vent valve (A) to cut of the atmosphere into the chamber and series valve (B) to connect the the vacuum pump to the chamber to create vacuum (4) Typical spectrum obtained in PC using CN-Spec software.

quantity of the isotope. Here, we are using non-enriched $Th(NO_3)$ powder obtained from chemical suppliers.

To begin with, let us choose the simplest setup with the chamber kept at atmospheric pressure. That is, the vacuum pump is switched off, and the vent valve is open.

3.1 Spectra of $Th(NO_3)$ obtained at Atmospheric Pressure:

In the first iteration, the experiment is performed by simply placing approximately $2gm$ of Thorium Nitrate powder inside the chamber at a distance of 2cm from the detector. The vacuum pump is switched off and the chamber is at atmospheric pressure. The data is acquired for a period of 2 hours and
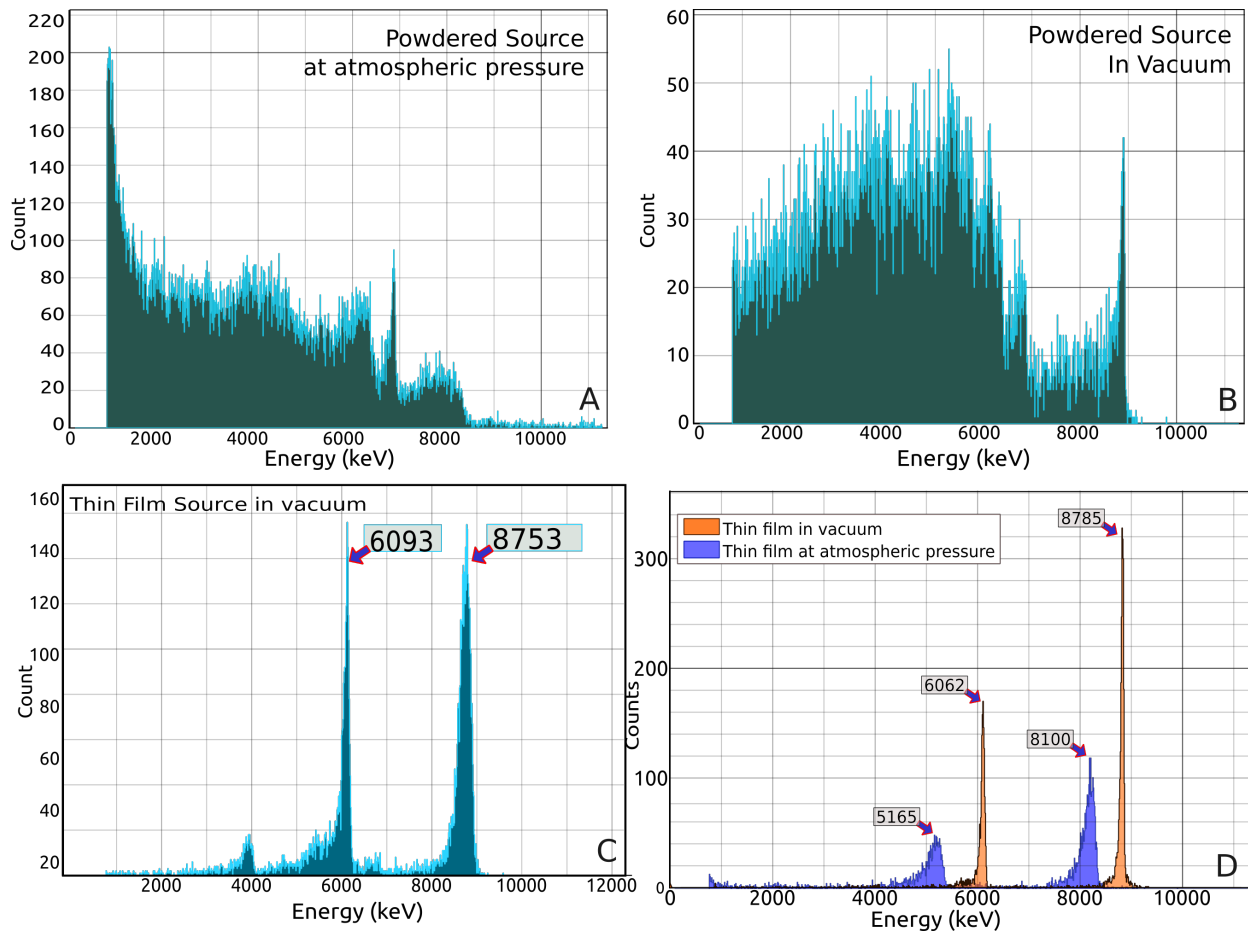
Figure 2: Radioactive sources under various attenuating factors; a) Alpha spectrum of Thorium nitrate salt; b) The same salt studied under vacuum; c) Thin film of ^{212}Bi under vacuum; d) Comparison of ^{212}Bi spectrum in 1 mbar vacuum and under attenuation due to 1 Bar atmospheric pressure.

the obtained spectrum is calibrated using manufacturer's data and is shown in Figure 2(a). The energy spectrum does not show well resolved peaks as expected from ^{232}Th given in Table-1, and is instead smeared over the entire region. A large build up of peaks appears at the lower end of the spectrum, that is, the cutoff/threshold energy. Certainly as a first guess, this loss in energy of alpha particles could be attributed to its interaction with air. So, the experiment is re-

peated with vacuum turned on.

3.2 Spectra of $Th(NO_3)$ obtained at 1 mbar Vacuum:

Again, 2gm of Thorium Nitrate powder is placed inside the chamber at a distance of 2cm from the detector. Following the instruction of the manufacturer, vent valve is closed so as to isolate the chamber from the atmosphere and the series valve is opened to

connect the chamber to the vacuum pump to evacuate the chamber slowly to reach 1 mBar pressure. The data is once again acquired for a period of 2 hours and the spectrum is shown in Figure 2(b). The large peak which was present near 800keV (channel 100) due to the minimum threshold setting has certainly been reduced and a sharper peak has appeared at the far side of the spectrum matching the expected 8785 keV line of ^{232}Th series. The rest of the spectrum is still an enigma. None of the other expected peaks are clearly defined and are all lost in a somewhat unexpected background. Now that the scattering losses due to air are minimized, the only interactions probably are due to the source itself. If the thickness of the source were large, then the lines of the spectrum are broadened to lower energies which is due to the interaction of alpha particles with various nuclei present along the various layers. This phenomenon is known as self-absorption. To reduce the losses due to self-absorption, we need to prepare a thin film source. There are different ways of preparing thin film sources and here we have chosen to prepare one using electrolysis.

3.3 Spectra of ^{212}Bi Source with Vacuum:

The process of preparing thin film sources using electrolysis is an open-ended experiment in itself. In the course of our efforts, we have realized that optimizing the electrolysis process has many parameters such as

- The amount of the salt in the aqueous solution (one can try other solvents) referred to as concentration.

- The type of electrode materials to be employed: Lead, Aluminium, Copper etc..

- The amount of constant current (typically in mA) to be passed through the solution, and the potential difference maintained between the electrodes.

- The time for deposition; typically a few minutes.

We have to vary only one of the parameters while keeping all others fixed, and perform the experiment to understand the causal relationship on the quality of obtained alpha spectrum. This has been taken up in a systematic fashion and the experiments lasted for almost a year. Here, we only present and analyse the results for the spectrum obtained by selective deposition of ^{212}Bi. In the initial trail for obtaining the thin film source, we have dissolved approximately 3 gm of $Th(NO_3).5H_2O$ in 5 gm of water and performed electrolysis with Lead (Pb) electrodes by passing 10 mA of current (with 450 mV potential difference) for 10 minutes. The obtained spectrum is shown in Figure 2(c). Here we have used the single point calibration using the data provided by the manufacturer for Am-241 source (5485 keV energy corresponding to channel number 495.6). We find that there are two

peaks, at 6093 keV and 8754 keV respectively. Clearly, the second peak corresponds to the decay of ^{212}Po. The first peak at 6093 keV is close to those from ^{212}Bi, but have not been resolved into separate peaks due to limitations of the instrument. Specifically, the FWHM of the Am-241 peak which was around 80 keV tells us that we must not expect to observe peaks with lesser spacing than this to be resolved.

3.4   Effect of air scattering on spectral lines:

To gain appreciation for the effect of energy loss due to scattering with air alone, the experiment is repeated with a second set of parameters for the thin film source prepared with 3.5gms of $Th(NO_3).5H_2O$ dissolved in 5 gm of water, using Pb electrodes and passing current of 19mA (with a potential difference of 350mV) for 10 minutes. The experiment is performed in two steps. Initially the spectrum is obtained with vacuum for 30 minutes duration and then the vacuum is turned off and then the vent valve is opened to release air into the chamber and obtain a second spectrum.

The orange colored histogram in Figure 2(d) corresponds to the energy spectrum of ^{212}Bi thin film in vacuum (1mbar) taken for 30 minutes, and after venting the vacuum and bringing the chamber to atmospheric pressure, the blue histogram was acquired. Care was taken to ensure that the total number of events recorded in both spectra are nearly

similar in order to make a comparable study. The effect of attenuation due to air can be clearly observed. Since we have already determined that the film deposited yields a majority of ^{212}Bi isotope, we can now use its known energies to apply a two point calibration to the spectrum. Since the lower energy peak seen around 6093 keV is a combination of two energies, a weighted average of 6062 keV has been considered for it. The higher energy peak has a known energy of 8785 keV. Both peaks have lost energy and shifted to 8100 keV and 5165 keV from 8785 keV and 6062 keV respectively. It can also be noted that the higher energy alphas have lost lesser energy as compared to the ones corresponding to the lower energy peak. The loss in energy corresponding to higher energy peak is 684 kev and to that of lower energy peak is 897 keV. This can be attributed to the fact that the higher energy alpha particles spend less time travelling through air, and therefore face a lower chance of getting scattered. The peak amplitudes have reduced from 157.54 to 47 for peak at 6062 keV and from 319.54 to 114 for peak at 8785 keV. As compared to the spectrum taken under vacuum, the sharp peaks previously observed have now spread over a lot more channels because scattering is highly probabilistic in nature, and the alpha particles undergo varying levels of scattering and subsequent energy loss depending on the number of air molecules encountered along the way. The lower energy peak has spread in a wider range of channels as

compared to the higher energy peak.

4   Results, Analysis and Discussion

To build the skills of argumentation, one of the important learning goals in lab work, we need to quantify the results in a representation that allows for comparison with the expected outcomes. In our experiment, firstly, we require to determine the energies of the various peaks obtained in the spectrum along with an uncertainty range so as to be able to compare with the expected values in Table-1.

4.1   Determination of Energies in the Spectrum:

The centroids of these peaks are determined by manually estimating the channel spread based on a Poisson distribution [16].

First, the channel/energy that consists of the highest number of counts, say N, is considered. Then, the standard deviation σ is given by $\sqrt{N}$. All neighbouring channels whose heights lie within $N \pm 2 * \sigma$ are considered to belong to that peak. Their mean gives the centroid 'E' of the peak. The number of counts in the peak corresponding to 'E' is taken as the maximum and then Full Width at Half Maximum (FWHM) 'ΔE' is determined. The resolution of the peak is given by 'ΔE'/E.

Now, consider the peak corresponding to that of Bi. The energy bin 6093 keV has the maximum no. of counts given by 156.

Therefore, $\sigma = \sqrt{156}$ which is approximately 12.5 and so, 2σ is 25. Now, all the energy channels consisting of upto 131 counts in the vicinity of 6093 are determined to be varying from 6082 keV to 6104 keV. The energy channel to the left of 6082 keV is 6071 keV and to the right of 6104 keV is 6115 keV. Hence, the centroid is determined as the average of 6071 and 6115, which is 6093 keV. The energies at which the no of counts drops to 78(half the peak values of 156) is 6015 keV on the left and 6148 on the right, whose difference is the FWHM with a value of 133 keV. The resolution for this peak is given by (133keV/6093keV)*100 = 2.1%. Performing a similar analysis for the ^{212}Po peak, we obtain the centroid as 8753 keV and FWHM of 254 keV, with a percentage resolution of 2.9%. The energies of Bi and Po along with the FWHM and % Resolution are tabulated in Table-2. These values are in agreement with the known energies which are 6061.71 kev and 8785 keV respectively, with corresponding relative percentage errors of 0.51% and 0.35%.

4.2   Determination of Intensities of the Peaks:

The intensity of a peak is determined by taking the total number of counts that have contributed to the peak as they are all supposed to be from the same alpha energy emitted by the source. To obtain the total number of counts, we need to choose an interval of energy channels that belong to the peak. This is done by taking twice the stan-

Table 2: The energies, FWHM, Resolution, Intensity and Branching ratio for the two peaks in inset of Figure 4 corresponding to ^{212}Bi and ^{212}Po are shown. The best values from ENSDF/Nuclear data tables are shown below in brackets:

Peak	Energy (keV)	FWHM (keV)	Resolution (%)	Intensity (Total Counts)	Branching Ratio (%)
^{212}Bi	6093 (6062)	133	2.1	1811	33.2 (35.94)
^{212}Po	8753 (8785)	254	2.9	3640	66.8 (64.06)

dard deviation(σ) value which corresponds to 90% of the area under the distribution. For the Bi peak, the energy interval is chosen as [5960,6226] and the summation feature gives us 1811 counts under the peak. Similarly, for the Po peak, we obtain the intensity within an interval of [8504,9012] as 3640 as shown in Figure 2. A 3σ spread would have included 99% of the area, however we have only taken 2σ because of the close proximity of other peaks from the thorium spectrum to the peak of ^{212}Bi decaying to ^{212}Tl which will affect the half life estimate if included.

4.3 Determination of Half-life:

Consider the spectrum, shown in inset of Figure-4, obtained for 4 hours with thin film prepared using the second set of parameters and placed in vacuum. It has two well defined sharp peaks and all the losses due to air scattering and self-absorption seem negligible. During the course of obtaining the spectrum, the intensities of both the peaks are saved after every twenty minutes for determining the half-life of Bi. Experimentally, the half life is determined by

measuring the activity of the source [17], which is defined as the number of decays per unit time, and is expressed mathematically as,

$$A(t) = \frac{dN_d(t)}{dt} \tag{1}$$

where

$$N_d(t) = N(0) - N(t) \tag{2}$$

is the number of radioactive decay at time t, N(0) is the radioactive nuclei at time t=0 and N(t) is the number of nuclei left in the sample at time t expressed as

$$N(t) = N(0)e^{-\lambda t} \tag{3}$$

where λ is the decay constant.
Hence activity can be further expressed as;

$$A(t) = \frac{dN_d(t)}{dt} = -\frac{dN(t)}{dt} = \lambda N(t)$$
$$= [\lambda N(0)]e^{-\lambda t} = A(0)e^{-\lambda t} \tag{4}$$

In our experiment, we determine the total number of counts I(t), obtained using the summation option in the software. These counts I(t) is directly proportional to the decayed nuclei per unit time, whose alphas have been registered by the detector at a
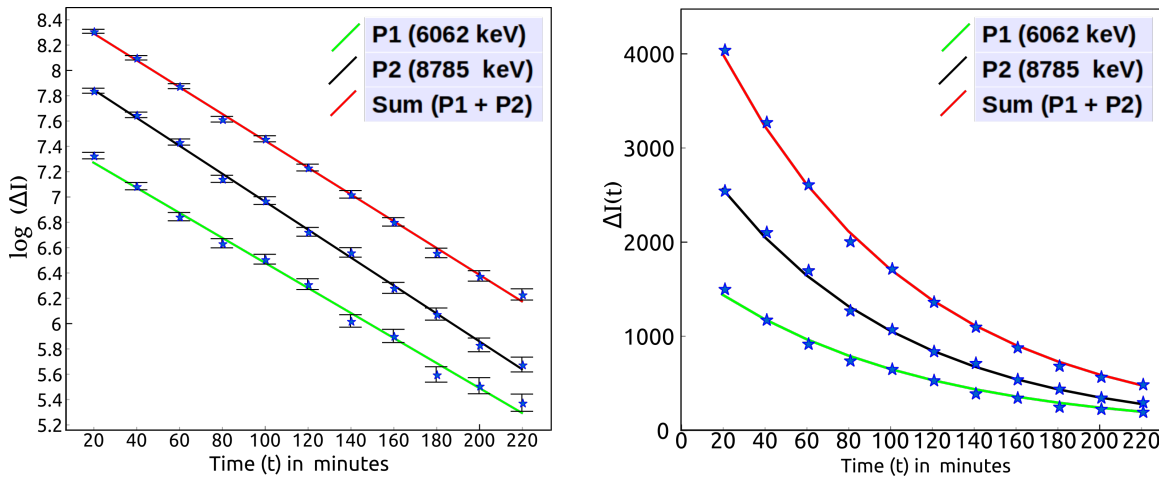
Figure 3: a) Log plots for counts per unit time obtained for both ^{212}Bi peaks as well as their sum in twenty minute intervals. b) Half life calculations for ^{212}Bi spectrum peaks at 6062 keV and 8785 keV using least square fit with a standard exponential decay function.

particular energy. The software's data logger utility saves these counts I(t) related to a peak at regular intervals of time Δt as specified by the user. Here, we have choosen to save the total counts in twenty minutes interval.

Now, approximating A(t) as $\frac{\Delta N_d}{\Delta t}$ (reflected as $\frac{\Delta I(t)}{\Delta t}$), we can rewrite eqn (4) as

$$\Delta I(t) = [\Delta t A(0)]e^{-\lambda t} = I(0)e^{-\lambda t} \quad (5)$$

where $\Delta I(t) = I(t + 20) - I(t)$ is the counts obtained in particular twenty minutes interval.

The counts data is obtained for the two peaks as P1 (6062 keV) and P2 (8785 keV) and their sum as Sum (P1+P2). The plots of $log(\Delta I)$ vs t fitted with linear regression are shown in Figure 3(a).

The decay constants given by the slopes of the respective lines are shown in Table 3. The observation that the three fitted lines are almost parallel reflects the fact that

the decay constant should remain the same through both the α and $\beta-$ branches [8]. The obtained decay constants are used to fit the actual data with exponential functions. This approach is followed because students can easily get confused by looking at the seemingly different exponential decay plots.

4.4 Uncertainty in Half-life

The half-life is given by $t_{1/2} = \frac{0.693}{\lambda}$. Hence, its uncertainty is $\delta t_{1/2} = \frac{0.693 * \delta\lambda}{\lambda^2}$. $\delta\lambda$ is obtained by determining the standard deviation in the slope of the regression data, given by:

$$\sqrt{\frac{\frac{1}{n-2}\Sigma_{i=1}^{n}(y_i - \hat{y}_i)^2}{\Sigma_{i=1}^{n}(x_i - \bar{x})^2}} \quad (6)$$

The obtained standard deviation for three regression data are tabulated in Table 3. The half-life and its uncertainty for each of the data is determined and presented in Table 3. The best value for half-life is found

Table 3: The curves P1 and P2 belong to Bi and Po respectively. The decay constants and their respective standard deviations from linear regression and the corresponding half-lives with uncertainties are presented below.

Data Set	Decay Constant (λ in 10^{-2} sec^{-1})	Standard Deviation in Decay Constant ($\Delta\lambda$ in 10^{-4} sec^{-1})	Half life ($t_{1/2}$ in minutes)	Uncertainty in Half−life ($\Delta t_{1/2}$ in minutes)
P1 (6062 keV)	0.99	2.62	70.08	1.87
P2 (8785 keV)	1.10	1.39	62.77	0.79
SUM (P1+P2)	1.06	1.38	65.45	0.85

to be 62.77 Min with an uncertainty of 0.79 Min from the data, corresponding to that of P2, and this is because the peak is well defined with no adjacent peaks as compared to P1 which has combination from overlap of other Thorium daughters. The overall half-life is slightly greater than the expected value of 60.5 min with an error of 3.66%. This is because the thin film source contains small quantities of parent products of 212-Bismuth resulting from the 232-Thorium series, which would to some extent replenish Bismuth nuclei within the sample over time.

4.5 Low Intensity Peaks in the Spectrum:

To observe the alphas being accumulated from other nuclei in the radiactive series of ^{232}Th, we magnify the counts axis by a factor of 35. The peaks corresponding to those expected from Table 1, are identified with respective letters in brackets, and their energies (determined using Poisson distribution) are indicated in Figure 4. The obtained energy values match with the predicted ones closely.

5 Conclusions

We have used a non-enriched radioactive source $Th(NO)_3$ salt in powder form to prepare a thin film source of ^{212}Bi using electrolysis.

The α spectrum obtained by placing the source inside the airtight chamber at 1mBar vacuum for a period of four hours, has two peaks at 6093 keV and 8753 keV with resolution of 2.1% and 2.9% respectively. They match the expected values for ^{212}Bi and ^{212}Po to an accuracy better than 1% . The half-life of ^{212}Bi is obtained by determining the activity over 20 minute intervals, and the best value obtained from the distinct 8753 keV peak is found to be 62.77 $\pm$ 0.79 minutes, which matches the expected value of 60.55 $\pm$ 0.30 minutes to an accuracy of 3.5%.

The other possibilities such as alpha-spectrum analysis by preparing different thin film sources and study of linear absorption co-efficients of different materials
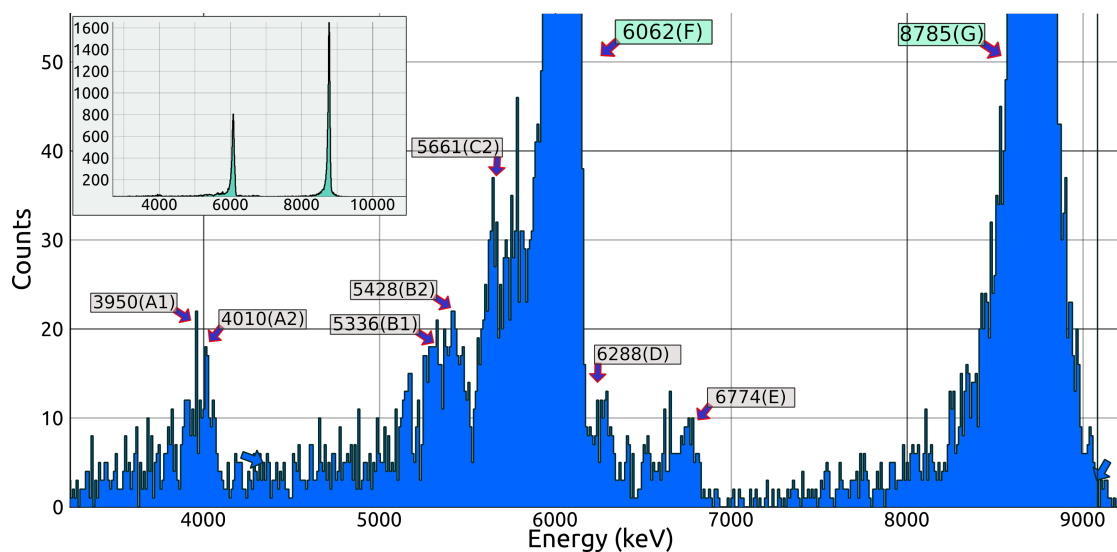
Figure 4: Spectrum obtained over a period of 4 hours from a thin film of ^{232}Th under 1mbar pressure showing prominent peaks for ^{212}Bi, as well as trace amounts of other isotopes. The spectrum has been expanded along the Y axis to exaggerate the small peaks formed by these trace isotopes. The complete spectrum is shown as an inset.

such as aluminium makes for exciting set of experiments for both UG and PG nuclear physics lab.

6   Acknowledgment

The authors thank Inter University Accelerator Centre(IUAC, New Delhi) for taking educational initiatives through their outrach programme, and providing a healthy environment for research and teaching in physics education.

References

[1] "Proposed syllabus and Scheme of Examination for B.Sc.(Honors) Physics" https://www.ugc.ac.in/pdfnews/7756304_B.SC.HONOURS-PHYSICS.pdf

[2] http://www.iuac.res.in/~elab/phoenix/experiments/mca.html

[3] https://csparkresearch.in/alphaspectrometer/

[4] Zwickl, Benjamin M., Noah Finkelstein, and Heather J. Lewandowski. "The process of transforming an advanced lab course: Goals, curriculum, and assessments." American Journal of Physics 81, no. 1 (2013): 63-70.https://aapt.scitation.org/doi/10.1119/1.4768890

[5] "Detailed Learning Goals for the Advanced Lab" http://spot.colorado.edu/~bezw0974/Resources/Detailed_LGs.pdf

[6] Martin, Brian R. Nuclear and particle physics: an introduction. John Wiley & Sons, 2006.

[7] Jithin et.al 'Measurement Model of an Alpha Spectrometer for Advanced Undergraduate Laboratories', Physics Education - January-March 2019.

[8] Krane, Kenneth S., and David Halliday. Introductory nuclear physics. Vol. 465. New York: Wiley, 1988

[9] Cohen, Bernard Leonard. Concepts of nuclear physics. Tata McGraw-Hill Education, 1971

[10] Patel, Shriprakash B. Nuclear physics: an introduction. New Age International, 1991.

[11] Hubsch, Tristan. "The theory of alpha decay." (1997)

[12] Evaluated Nuclear Structure Data File Search and Retrieval, NNDC, Brookhaven National Laboratory. https://www.nndc.bnl.gov/ensdf/

[13] Dong, Tiekuang, and Zhongzhou Ren. "New calculations of α-decay half-lives by the Viola-Seaborg formula." The European Physical Journal A-Hadrons and Nuclei 26, no. 1 (2005): 69-72.

[14] "Gamow's Theory of Alpha Decay" https://fenix.tecnico.ulisboa.pt/downloadFile/3779576931836/Ex8Serie1/

[15] Tuli, Jagdish K. "NUCLEAR WALLET CARDS." (2011).

[16] 'Study of Alpha-energies of Radium-226' http://web.vu.lt/ff/a.poskus/files/2013/06/NP_No11.pdf.

[17] Determining the half-life of Ba137 http://www.kau.edu.sa/GetFile.aspx?id=258656&fn=01%2020Half%2020Life.pdf

[18] Giordano, Nicholas J. Computational physics. Pearson Education India, 2006.

Measurement Model of an Alpha Spectrometer for Advanced Undergraduate Laboratories

B.P. Jithin[1], V.V.V. Satyanarayana[2], Swapna Gora[1], O.S.K.S Sastri[1*] and B.P Ajith[2]

[1]Dept of Physics, Central University of Himachal, HP 176215, India.
*sastri.osks@gmail.com

[2]Inter University Accelerator Centre, Delhi, India.
ajith@iuac.res.in

Submitted on 03-08-2018

Abstract

In this paper, we present the modeling aspects relevant to students at the advanced UG level for using an Alpha Spectrometer as a measurement tool for nuclear physics experiments. The four stage modeling methodology for construction of theoretical models is utilised as a framework to understand the various aspects of an alpha spectrometer. The presentation specifically focuses on alpha spectrometer '**AlphaSpec-1K**' indigenously designed and developed by us. The spectrometer output is interfaced to the USB port of a PC, and the associated software '**CNSpec**', which is licensed under open-source terms, has built-in features to fit, calibrate, and perform various analysis of the obtained spectrum. The spectrometer is designed to detect alpha energies in a full scale range of 10 MeV with a resolution of 81 keV at 5485 keV. It is calibrated using ^{241}Am and tested for linearity using ^{229}Th multi-peak source, and as a final step, has been validated using ^{212}Bi, by verifying its spectrum with published literature, as well as calculating its half life to better than 1% accuracy.

1 Introduction

One of the major goals in imparting physics education is to incorporate good laboratory practices alongside theoretical modeling and computer simulation based approaches. Physics Education Researchers have deliberated on various aspects of laboratory practice such as learning goals for advanced physics labs [1], cognitive task analysis [2], lab environment with regards to engagement of teachers and students in lab activities [3], and the mode of assessment [4]. Especially, the PER group at Colorado, Boulder has developed a set of learning goals for physics laboratories [5], wherein

emphasis is laid on measurement models. They contend that modeling the measurement process is important since the instrument should not merely remain a black box for the students and that they should understand the principles of operation, key model parameters, and limitations pertaining to the ideal functioning of the apparatus. Our PER group, in collaboration with the teaching lab of the outreach cell of IUAC New Delhi, is focussing on developing lab experiments for nuclear physics along with activities, simulations, and demonstrations to go hand-in-hand with the theoretical course. As a part of this effort, we are in the process of developing experiments based on Geiger counters, as well as gamma and alpha spectrometers, where in we have two primary goals:

1. Design and development of low cost alpha and gamma spectrometers

2. Design and development of nuclear physics experiments using non-enriched sources

A key area of focus is the effective implementation of these outcomes in labs through the application of PER practices. We have submitted a paper [6] to the same journal, wherein we have discussed an experiment to study the alpha spectrum and half-life of ^{212}Bi. The Bi source was prepared using electrolysis of non-enriched $ThNO_3$ powder and the spectrum is obtained using our indigenously developed alphaspectrometer '**AlphaSpec-1K**'[7].

Modeling the measurement apparatus and familiarisation with its usage are crucial precursors to actually utilising them to perform experiments. Here, we utilise the modeling theory structure suggested by Hestenes [8] which has been employed almost as a methodology. Its inherent design helps systematise our understanding of the scientific process of learning, as it is very effective in applying the constructivist pedagogy wherein students are guided (typically using the Socratic method) to build their understanding of the current topic based on their previous knowledge. Even though the modeling theory suggested by Hestenes is for constructing theoretical models, we have used the same technique to model the measurement apparatus, here the alpha-spectrometer '**AlphaSpec-1K**' by using the tools of an experimentalist instead of those of a theoretical physicist. In the next section, we give a brief outline of the four stages in the modeling structure with reference to the alpha spectrometer, and in subsequent sections, discuss the various stages in detail with focus on experimental aspects such as characterisation,calibration, and data collection.

2   Modeling the alpha spectrometer

In order to build the alpha spectrometer, one needs a sensor (a transducer along with the required electronics) that detects the energy of the alpha particles and outputs a

proportional voltage signal. In this section, we model the detection process in tune with the modeling theory proposed by Hestenes [8] which has the following four stages.

1.Description Stage: Here, we describe
(i) the object which is the detector,
(ii) the process involved, that is, creation of charge pairs within the depletion region, and finally,
(iii) the interaction responsible for creation of charge pairs when alpha particles deposit their energy in the depletion region.

2.Formulation Stage: While the theoretician formulates the laws and principles involved with regard to the process and interaction, the experimentalist focusses on the detection procedure, which involves the following three steps:

(i) capturing the alpha particles without any loss of their energy prior to entering the detector's active volume

(ii) converting the alpha energy into a measurable voltage through various signal processing electronic circuits

(iii) acquiring the data by a computer for visualization of the spectrum, and for subsequent statistical analysis

Even though our approach involves construction of the apparatus from an experimental design perspective [2], from the modeling perspective it suffices to deal with understanding the principles and reasoning

behind the need for various aspects of the apparatus design. Even though this understanding would help in troubleshooting a malfunctioning apparatus, it might not enable carrying out repairs. From a researcher's point of view, careful insight into the measurement process enables proper identification of any anomalies in the final spectrum output. This is an important learning goal.

3.Ramification Stage: From a theoretical perspective, this stage involves solving the equations related to the model object and obtaining the emergent properties in a form that can be compared with experimental outcomes. From an experimental angle, this stage can be termed the testing part, which is also an important learning goal for advanced laboratories [5]. For the measurement model, this stage involves studying the manufacturer's data with regard to usage of the apparatus. In the case of the alpha spectrometer, this involves obtaining the spectrum and calibrating it to obtain the emergent properties such as energy and intensities of the peaks.
Typically, the manufacturer performs experimental runs in which the apparatus along with the detection system is tested with a well known α source such as ^{241}Am, and then specifies the calibration procedure for converting the channel number into useful energy information. Further, the apparatus is tested for understanding the effect of source-detector distance, and also that of

Figure 1: The object, process and interaction are described in detail with relevant diagrams alongside
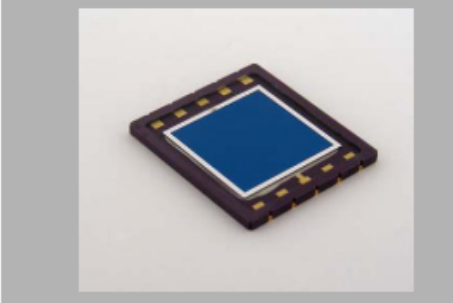
OBJECT	
Object	Sensor/Detector
Type	PIN Photodiode
Composition	Silicon
Object Variables	Area: 10mm x 10mm Circular Collimator Diameter : 8mm
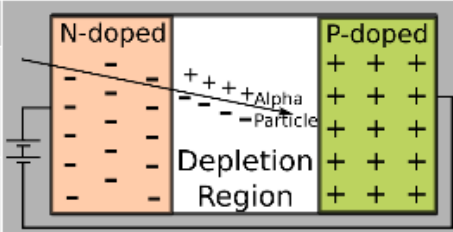
PROCESS	
Reference System	Depletion region of the PN Junction acts as the sensitive volume of the detector
State Variables	Number of charge pairs formed (N)
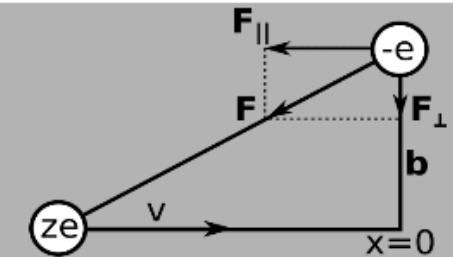
INTERACTION	
Interaction Type	Ionisation
Agent	Alpha Particles
Interaction Variables	Reverse Bias Voltage (VRB)

air pressure on the obtained spectrum to finalise the ideal vacuum for experimentation. Finally, the detection system is tested for linearity by using a source of ^{229}Th which has distinct multiple peaks with known values that can be easily resolved. In the current paper, these are discussed as part of the ramification process, as these could be performed by the students in the lab as well, given the availability of enriched sources of ^{241}Am and ^{229}Th. We also intend to make this a part of the familiarisation procedure by implementing this

testing and calibration phase using ^{212}Bi, a non-enriched source prepared using the electrolysis process discussed in [6].

4. Validation Stage: The obtained outcomes (emergent properties) are validated with known predictions by using either theoretical considerations, or previously known experimental results. The apparatus is now ready for experimentation with other sources for validation, and to undertake research with unknown sources.

In the following four sections each of these

stages is discussed in detail with appropriate flow diagrams and results.

3   Description stage

a) Principle of operation: Typically an alpha detector consists of a semiconductor PN junction connected in reverse bias mode so as to create a depletion region that acts as an ionisation medium to convert the alpha particle energy into electron-hole pairs which move towards the electrodes due to the applied electric field. The small amount of charge generated as a result of one alpha particle depositing its entire energy in the depletion region is proportional to its energy, and this charge is a measurable quantity.

b)   Description of the detector: The **type** of detector that we have employed is a PIN photodiode whose **composition** is Silicon. The detector (**dimensions** specified by the manufacturer [7]) has $10mm \times 10mm$ surface area and $5mm$ thickness. In front of the detector is a circular collimator of 8mm diameter whose purpose is to prevent alpha particle incidence near the boundary of the detector where its behaviour is non-linear and results in erroneous readings.

c) Description of the Process: The PIN photodiode is connected in reverse bias so that a depletion region of the junction is created. The reverse bias voltage (V_{RB}) is chosen such that the width of the deple-

tion region is maximum, and hence the active volume of the detector is maximised. This also reduces the junction capacitance and thereby reduces noise. The current produced due to a voltage V_{RB} across depletion region width l is given by [9].

$$I = nq\mu_n \frac{V_{RB}}{l} \tag{1}$$

Where n is the number of charges (q) generated in the depletion region, and μ_n is the mobility of the charge carriers. μ_n is typically constant for low V_{RB} . The electric field across the junction is given by $E = \frac{V_{RB}}{l}$. The number of charges (n), is the **state variable** associated with the process.

d) Description of Interaction: The **type** of interaction responsible for creation of electron-hole pairs is ionisation within the depletion region. The **agent** of interaction is the coulomb force between the charged particles and electrons in the neutral material available in the depletion region. An alpha particle (positively charged) with sufficient kinetic energy (implying large velocity) exerts a coulomb force on the electrons in the atom (Figure 1) to escape from the atom, or atleast take it to one of the excited states (leaving the atom in its excited state). The amount of ionisation due to the incident alpha particle of energy E_α is going to be dependent on the active volume available for the particle to completely deposit its energy (a depletion region of width $10\mu m$ should suffice), and in the process, create an equivalent number of electron-hole pairs.The
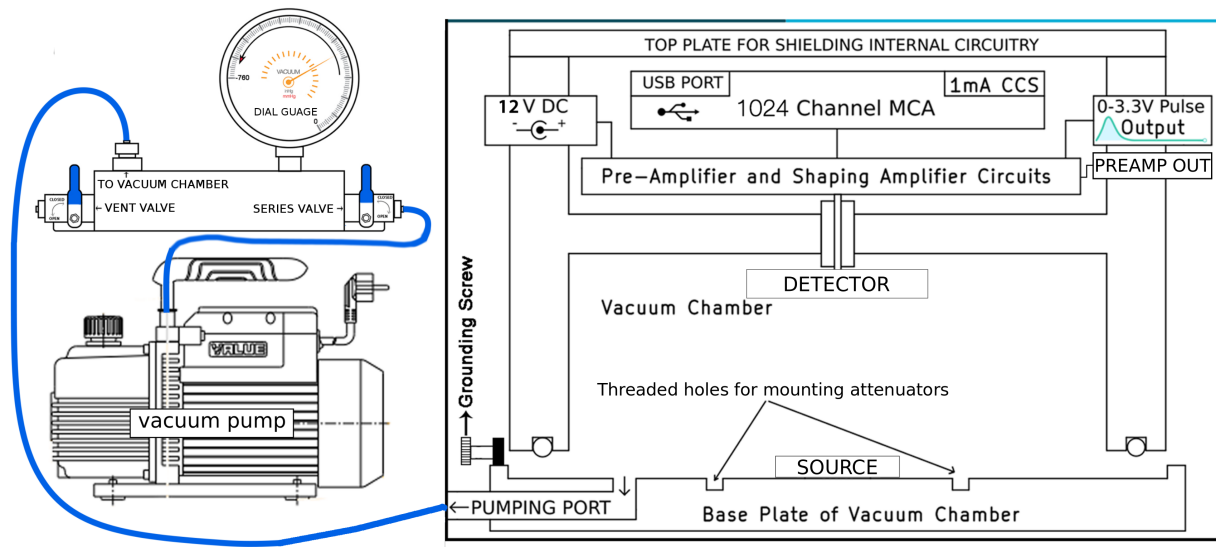
Figure 2: Source-Detector Enclosure Design along with the Vacuum pump and its assembly

energy required to create on electron-hole pair in silicon is 3.62eV, so the total number of pairs generated can be estimated based on the initial energy of the alpha particle. So, the **interaction variable** that affects the process is V_{RB}, which is responsible for the depletion region of thickness l.

4 Formulation stage

a) Enclosure design and Vacuum assembly: The first step is to ensure that only the alpha particles emitted by the source reach the detector without any loss of energy, and that they deposit their entire energy in the detector's active volume to generate a corresponding signal. The sensitivity of the detector to light photons necessisates placement of the source and detector inside an opaque enclosure. The enclosure is de-

signed to be air tight so that vacuum can be created within it to avoid loss of energy of alpha particles due to scattering with air. The design of the chamber along with the vacuum pump and accesories are shown in Figure 2.

The second step involves various stages of processing the signal to obtain the final spectrum reflective of the number of charge carriers deposited at various energies, and is outlined in the form of a block diagram in Figure 3 which is discussed below:

b) Conversion of charge to voltage: The signal from the detector is available as the number of charge carriers that have reached the electrodes, which is then converted into a corresponding output voltage by utilising a charge sensitive preamplifier. The main role of the preamp is to ensure impedance matching between high impedance at the detector side (i.e. input), with the low
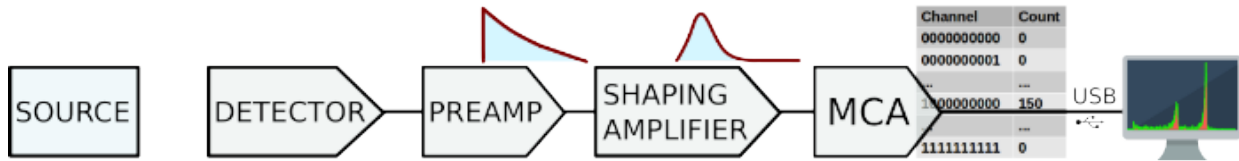
Figure 3: Signal Processing Electronics: The step by step process of conversion of alpha energy into a measurable quantity such as voltage that maintains a predictable proportionality is indicated as a flow diagram

output impedance of the post-processing electronics. This also improves the signal-to-noise ratio (SNR).

In this spectrometer, the designed preamplifier (open source hardware available at [10]) has a MOSFET at the input in cascade with a bipolar junction transistor (BJT) . A feedback capacitor present in the preamp is used to decide the gain/charge-sensitivity. A high value resistor (typically $100M\Omega$) is connected in parallel to discharge the capacitor (1pF) . In principle, an alpha particle of 1MeV energy should give a total charge ($Q = \frac{1*10^6*1.6e^{-19}}{3.62}$) [9] and the output voltage of the preamplifier is given by $V = \frac{Q}{C} = \frac{1*10^6*(1.6*10^{-19})}{3.62*(1*10^{-12})} = 44.2mV$.

To study the output characteristics of the preamplifier, we have chosen ^{241}Am as the alpha source since it has a single alpha emission at $5.485MeV$ energy. As per our calculations, we should obtain about 242 mV as the peak voltage of the corresponding output from the preamplification stage, but due to the non-zero capacitance of the detector, the measured voltage was in the range of 150-200mV.

The preamplifier output provided in Figure 4 as H is for visualization purposes only as it has been attenuated by buffering circuits, and is not indicative of the actual output value. The rise time is determined to be close to 50nS, and it takes nearly 1mS to drop to 50% of its peak value, thereby giving it a distinct sawtooth appearance.

Because of these very short rise and fall times, the output voltage signal of the preamp cannot be easily digitized, and we need to process the signal further, which is done using a shaping amplifier.

The output of the shaping amplifier is also available via a BNC socket for external monitoring with an oscilloscope or a separate MCA. The maximum height of output pulses has a range of 0-3.3V, where 0 indicates the absence of a pulse, and 3.3V indicates an incident alpha particle with energy close to the maximum permissible value of 10MeV. The shaping amplifier [11] has a differentiator circuit followed by a second order active integrator to obtain a near gaussian pulse as shown in 4 as I. The peak value of this pulse is to be sampled and digitized.

c)   Digitization of the voltage signal:
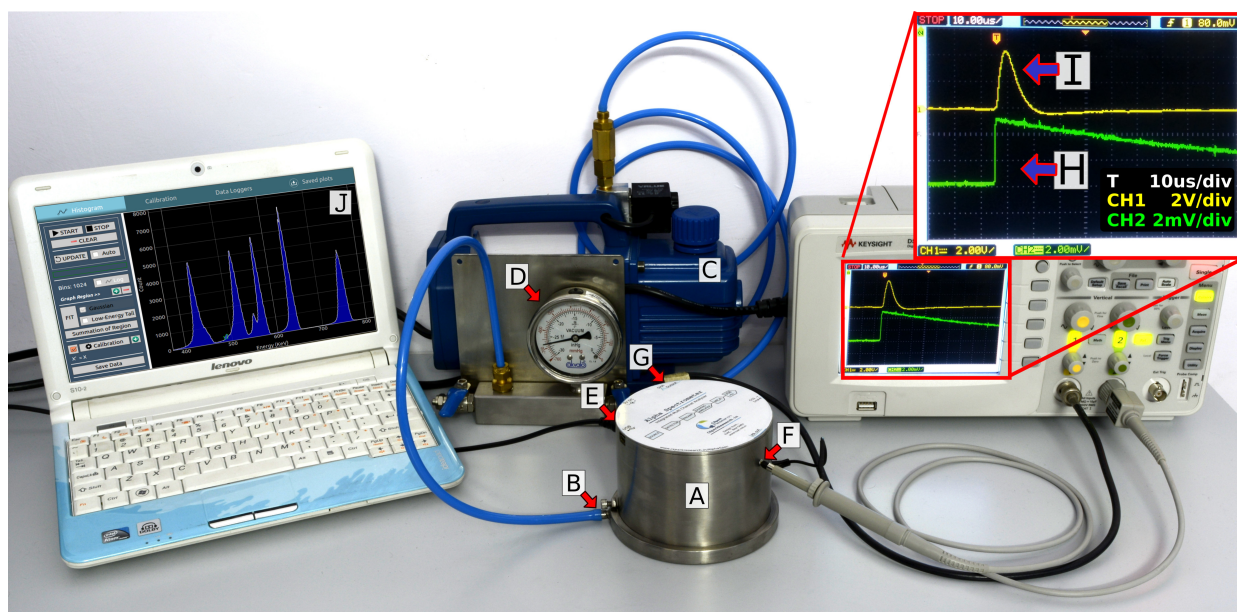
Figure 4: Entire experiment setup of the Alpha Spectrometer '**AlphaSpec-1K**' showing the source-detector enclosure(A) connected via the vacuum inlet port(B) to the pump(C), with pressure monitoring by a dial guage(D). It is connected to a laptop(J) via the USB port(E). Signal outputs from the pre-amplifier(F) and shaping amplifier(G) are connected to a 50MHz oscilloscope where the nature of these signals are shown as traces (H) and (I) respectively. The time scale of the oscilloscope is $1\mu S$/div, and the voltage scales for preamp and shaping amplifier are 2mV/div and 2V/div respectively. Signals have been offset for clarity.

The pulse is accepted if the amplitude is greater than the threshold value (to avoid very low energy peaks which might not be due to alpha particles) which is set to 50mV. The combination of peak detector and Analog to Digital Converter (ADC) is designed to convert the peak height (i.e. proportional to detected alpha energy) into a digital number, and the histogram data of energy vs number of counts is generated with the help of a Multi Channel Analyzer (MCA). The MCA is designed to have 1024 channel(1K) resolution, with an input voltage range of $0 - 3.3V$. This limits the energy resolution to $\frac{10MeV}{1023} = 9.7keV$.

d) Spectrum: The alpha spectrometer hardware performs a variety of tasks ranging from detection of the pulse, post-processing of the signal, and also sorting the signals on the basis of their peak height into predefined bins by the MCA. This information consisting of a table of number of pulses registered in each channel is stored in the in-built microprocessor of the MCA in a linear array, and must now be transferred into a computer via the USB communications port in order to visualize, analyse, and interpret the data.
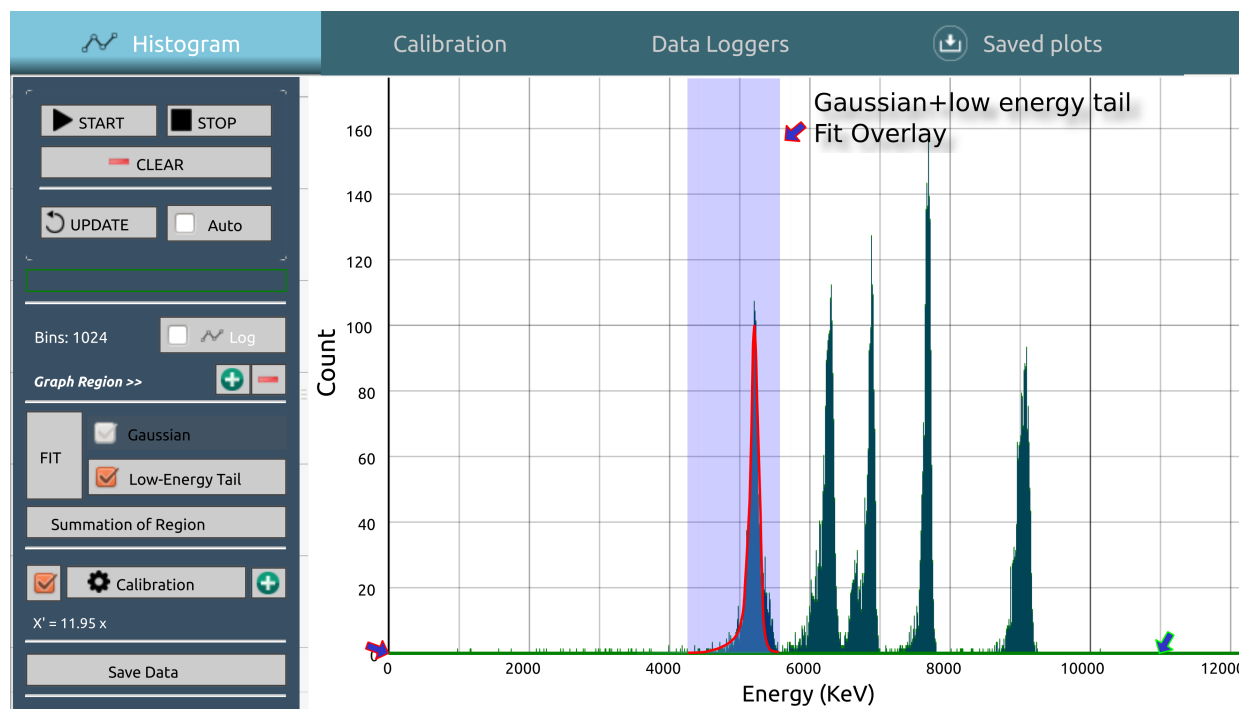
Figure 5: A Screenshot of the open-source software provided with the Alpha Spectrometer '**AlphaSpec-1K**':

e) <u>Housing the electronics</u>: Considering the highly sensitive nature of the signals from the detector, it is important to place the preamplifier very close to the detector to avoid noise and leakage. Equally important, is the need to house the signal processing electronics in an electrically shielded enclosure. To ensure this, a cylindrical structure segmented along the central plane via a 3mm stainless steel sheet was designed 2, and one segment was made vacuum tight with provisions for a sealing gasket and an inlet port for a pump as shown in Figure 2. The detector is electrically connected to the signal processing electronics via a very short (5mm) feedthrough which is

also vacuum tight. With this design, we have effectively placed all electronics in a Faraday cage.

f) <u>Software:</u> The final step is to implement a software that shall plot the acquired data in real-time and have utilities for data analysis. The open-source software **CN-Spec** written in the Python programming language employs a variety of powerful utilities such as Numpy, Scipy, and PyQtGraph for various mathematical and visualization purposes. It acquires the data from the hardware, and plots it in the form of a histogram showing channel number (corresponding to peak voltage proportional to alpha energy) on x-axis, and the number of charged parti-

cles received at each channel on the y-axis, as shown in Figure 5. The key analytical features incorporated as of now in the software are calibration using polynomials up to 2 orders, fitting with Gaussian plus low-energy tail (Lorentzian part) to obtain peak information, and a summation utility to obtain the total number of counts corresponding to a peak.

5   Ramification

Once the spectrum is available, the detection system is in principle ready for experimentation. But first, the proportionality constant between alpha energy and corresponding peak voltage obtained needs to be determined. This process is called calibration.

5.1   Calibration using ^{241}Am

When we place the ^{241}Am source, the α-energy spectrum corresponding to it must now appear as number of counts building up around a particular channel number. To determine the appropriate vacuum to be established for effectively neglecting the energy loss due to scattering, we perform the following two steps.

i) To study the effect of source-detector distance at atmospheric pressure:
The ^{241}Am source was placed at a distance of $25mm$ from the detector, and the average channel number (corresponding to energy) of its lone peak was measured. For this, we have implemented a least square fit routine which uses a standard gaussian

function, and record the centroid value (average channel number) for each dataset. The source-detector spacing referred to distance, was reduced in steps of 3mm and the centroid was noted for each distance. In the distance versus channel number plot shown in Figure 6(a), the linear dependence of energy loss with source-detector distance at atmospheric pressure demonstrates that the scattering of alpha particles is proportional to the distance travelled in air.

ii) To study the effect of air pressure:
The ^{241}Am source was placed at $30mm$ from the detector. The vent valve was closed, and the pressure inside the chamber was slowly decreased from 1000mbar to 100mbar in steps of 100mbar. The average energy of the peak that accumulates at a particular channel number is obtained at various pressures and plotted in Figure 6(b). At 200mbar itself, the peak energy is obtained at channel 469 which corresponds to placing the source at a distance of 3mm from the detector as shown in the previous section. That is, at 200mbar, the scattering losses are almost negligible. Further reducing the pressure to 50mbar is equivalent to placing the source almost in contact with the detector.

The final spectrum obtained by placing ^{241}Am at a distance of 2 cms and a pressure of 50 mBar is shown in Figure 6(c). The centroid of the spectrum is found to be located at channel number 496 via a gaussian fitting routine, and since the energy of this peak is well known to be at 5485 keV, one can fit a
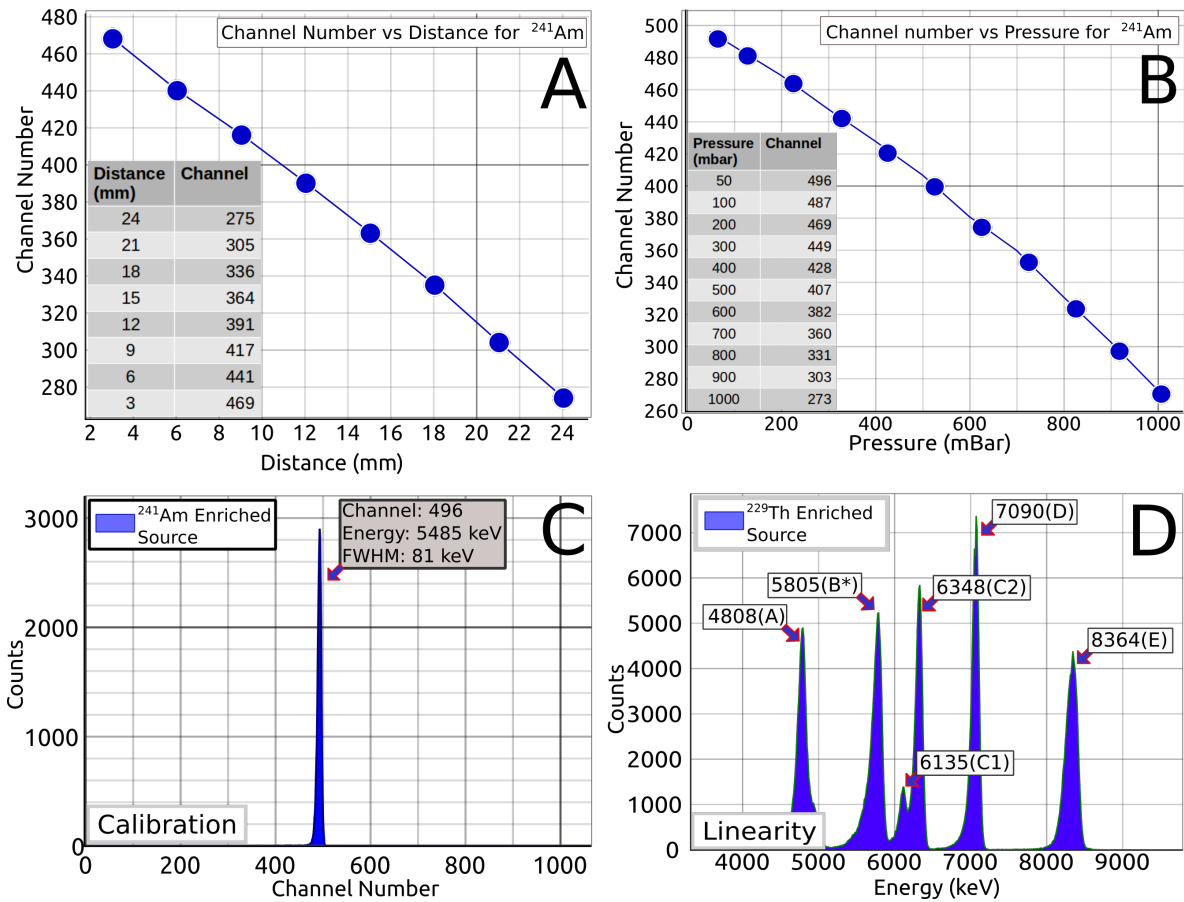
Figure 6: a) Effect of source-detector distance on the centroid of the lone peak of ^{241}Am. b) Effect of air pressure is studied for the same centroid . c) Alpha spectrum for ^{241}Am under 50mBar vacuum with source-detector distance = 2cm . d) Alpha spectrum for ^{229}Th under similar conditions as in (c)

calibration polynomial as follows:

$$Energy = \frac{5485}{496} \times channel\,number \quad (2)$$

An FWHM of 81 keV was obtained via a gaussian fit of the calibrated peak. ^{241}Am enriched source is commonly employed for single point calibration purposes since it produces a single peak at a known energy. However, since single point calibrations are not equipped to correct offset errors, it is advisable to use a source with at least two decay processes with alpha particle emissions

at known energies, such as ^{212}Bi. We can now cross-check if our calibration remains linear over the entire range of 10 MeV. A good source for checking this is the multi-peak source ^{229}Th whose energies are compiled from ENSDF and shown in Table 1.

5.2 Linearity check using ^{229}Thorium

To verify the linear energy response of the detector, a ^{229}Th source is placed at 20 mm from the detector and the data is acquired

Table 1: The radioactive decay chain of ^{229}Th with alpha energies (with intensities more than 5%) and their respective intensities are compiled from ENSDF. The beta decays are also shown for the sake of completeness.

Parent	Daughter	$E\alpha$	$I\alpha$	$t_{\frac{1}{2}}$
^{229}Th	^{225}Ra	4845.3(A)	56.2	7340y
		4814.6	9.3	
^{225}Ra	^{225}Ac	β	-	14d
^{225}Ac	^{221}Fr	5830 (B*)	50.7	10d
		5732	8	
		5790.6	8.6	
		5792.5	18.1	
^{221}Fr	^{217}At	6126.3(C1)	15.1	4.9m2
		6341(C2)	83.4	
^{217}At	^{213}Bi	7066.9(D)	99.9	32.3ms
^{213}Bi	^{209}Tl	5869	93	45.59m
^{213}Bi	^{213}Po	β	-	45.59m
^{213}Po	^{209}Pb	8375.9(E)	100	4.2us
^{209}Tl	^{209}Pb	β	-	2.2m7
^{209}Pb	^{209}Bi	β	-	3.25h14

under a vacuum of 50 mbar. The obtained spectrum, shown in Figure 6(d) has been calibrated, and the peaks correspond to their expected energies with an accuracy better than 1%. The peak $B*$ in Figure 6 corresponds to four values shown in Table 1. Since these peaks have energies too close to be individually resolved by the current spectrometer, we assigned their weighted average of 5817 keV to be the expected value for $B*$. The accuracies of the obtained energies confirms that the linearity of the detector is assured over the full scale range of the instrument to better than 1% .

6 Validation
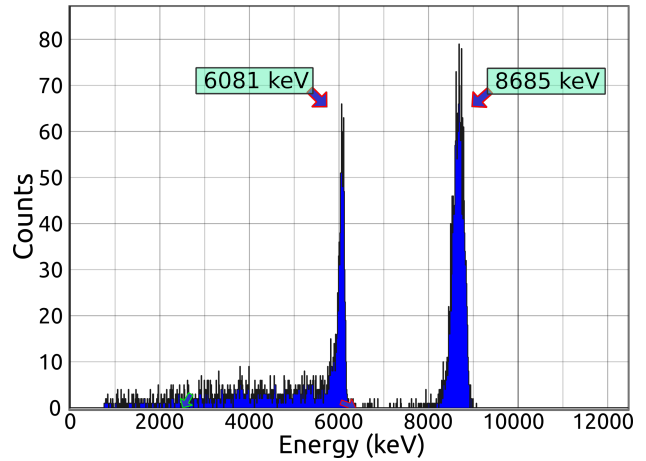
Figure 7: ^{212}Bi Spectrum
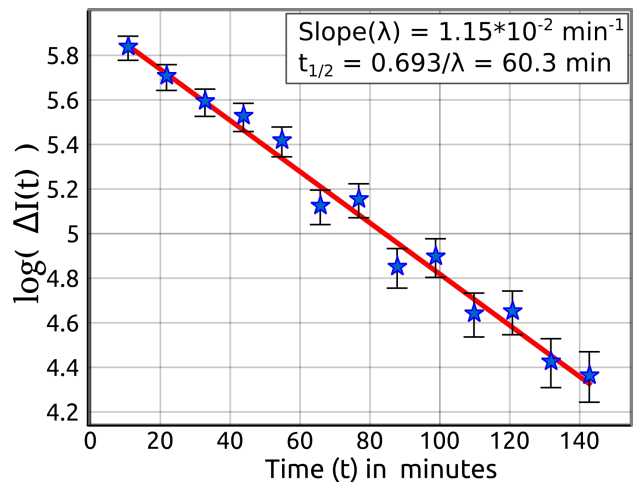
Figure 8: Log of activity of ^{212}Bi recorded as a function of time for calculating its half life

In order to validate our instrument, we must now record the spectrum from a third source, and verify that it matches with known values. For this purpose, we have prepared an un-enriched source of ^{212}Bi extracted from Thorium Nitrate salt via elec-

trolysis. The extraction procedure is carefully documented by Swapna et al [6], and their results also include spectrum characterization as well as half-life calculations.

In order to extract Bismuth, 3.5gms of Thorium Nitrate($ThNO_3$) salt was dissolved in 5gms of water. Electrolysis of this solution using 20mA current and lead foil electrodes for 10 minutes yielded a greyish film on both electrodes. The anode was placed in the vacuum chamber at a distance of 1cm from the detector to acquire the spectrum.

It had two distinct peaks with centroids at 6081 keV and 8685 keV as shown in Figure 7. These values correspond closely with the known energies from the decay chain of ^{212}Bi which are 6062keV and 8785keV [6] with percentage errors of 0.31% and 1.13% respectively.

Since the peak formed around 6081keV may also contain contributions from various trace isotopes from the Thorium-232 series as explained by Swapna et al[6], we used the higher energy peak formed around 8685keV for half-life calculations.

The activity was obtained by determining total counts under the 8685 keV peak in 12 minute intervals. The log of the activity has been plotted as a function of time in Figure 8. The slope of the regression line determines the decay constant λ(shown in inset of Figure 8) using which the half-life is determined to be 60.3 minutes with an uncertainty of 2.4 minutes. It agrees with the expected value of 60.5 minutes to an accuracy of 0.33%.

7 Conclusions

We have presented the way to model an alpha spectrometer, **AlphaSpec-1K** developed by us, so as to familiarize students with:

- the basic principles involved in the detection process (theoretical aspects)

- the need for various parts of the spectrometer (design aspects)

- the outcomes at various stages (troubleshooting aspects)

- the way to calibrate it and test for its linearity (analysis aspects) and finally

- perform experiments using it (application aspects)

To help develop a structured approach, we have utilised the framework proposed by Hestenes for actualising theoretical models and have applied it to modeling a measurement apparatus such as an alpha spectrometer.

8 Acknowledgment

References

[1] W. K. Adams and C. E. Wieman, "Development and validation of instruments to measure learning of expert-like thinking," *International Journal of Science Education*, vol. 33, no. 9, pp. 1289–1312, 2011.

[2] C. Wieman, "Comparative Cognitive Task Analyses of Experimental Science and Instructional Laboratory Courses," *The Physics Teacher*, vol. 53, no. 6, pp. 349–351, 2015.

[3] A. Hofstein and V. N. Lunetta, "The laboratory in science education: Foundations for the twenty-first century," *Science education*, vol. 88, no. 1, pp. 28–54, 2004.

[4] E. Etkina, S. Murthy, and X. Zou, "Using introductory labs to engage students in experimental design," *American Journal of Physics*, vol. 74, no. 11, pp. 979–986, 2006.

[5] C. Boulder, "Detailed Learning Goals for the Advanced Lab,"

[6] Gora Swapna, B. Jithin, V. Satyanarayana, O. Sastri, and B. Ajith, "Alpha Spectrum of ^{212}Bi Source Prepared using Electrolysis of Non-Enriched ThNO$_3$ Salt,"

[7] CSpark Research, "Alpha Spectrometer (AlphaSpec1K)."

[8] D. Hestenes, "Foundations of Mechanics," 1998.

[9] ORTEC, "Preamplifier and Amplifiers," tech. rep., 2015.

[10] B. Ajith and V. Satyanarayana, "Alpha Spectrometer."

[11] M. Sanchez-Raya, J. A. Gomez-Galan, E. Cojocaru, M. P. Carrasco, R. J. Naharro, F. M. Chavero, and I. M. Bravo, "Linear tunable analog front-end electronics for silicon charged-particle detectors," *IEEE Transactions on Instrumentation and Measurement*, vol. 64, no. 2, pp. 418–426, 2015.

Breakdown of Dimensional Analysis in Physics

Debnarayan Jana[1]

[1]Department of Physics, University of Calcutta

92 A P C Road, Kolkata- 700 009, West Bengal, India.

`djphy@caluniv.ac.in`

Abstract

Dimensional analysis (DA) provides us a very simple heuristic method to solve the dependence on the variables without invoking much theoretical knowledge. Moreover, this technique is of great help to experiments because it eventually serves as a guide to the key parameters which influence the phenomenon. However, there are situations in physics where there is a breakdown of this dimensional analysis. We indicate few examples from classical mechanics, electromagnetism and statistical mechanics. We briefly point out the reasons behind such breakdown of such successful tool in theoretical physics.

Keywords: Dimensional Analysis, Damping Force, Vector potential and Magnetic field, Critical Phenomena

1.Introduction

Dimensional analysis (DA) is nothing but a mathematical technique [1, 2, 3, 4, 5, 6, 7] used generously in physical science, chemical science and technology to study the dimensions of physical quantities and correctness of equations. This mathematical technique is most suitable in research work for design and conducting model tests. Even in bilological sciences, there are interesting ways of looking to the problems via this technique [8, 9, 10, 11]. For some interesting applcation of DA in quantum physics and other related problems, we refer to the literature[12, 13, 14]. In DA, one first predicts the physical parameters which will influence the problem and then by grouping these relevant parameters in appropriate dimensionless combinations; one can get a better understanding of the problem.

The paper is organized as follows. We first present a problem from classical mechanics where there is breakdown of DA. In section 3, we present a very well-known problem from classical electromagnetism which may serve as a key to regularization and renormalization in field theory. In the last problem we point an apparent violation of DA

in critical phenomena. In section 5, we give our conclusions.

2.Examples from Classical Mechanics

Suppose we are interested [15] to find out the stopping distance and time required for a point particle having mass m with an initial speed V_0 under a damping force given by $F = bv^n (n \geq 0)$. Before we analyze the problem from Newton's equation of motion, we would devote ourselves to look for the solution from pure dimensional analysis. The problem contains three parameters apart from the mass m of the particle, one being dimensionless number $[n] = M^0 L^0 T^0$ and another two are $[b] = [ML^{1-n}T^{-2}]$ and $[V_0] = [LT^{-1}]$. We can now construct the distance S travelled before the particle stops and the t required to stop. It is easy to visulaize that

$$
\begin{aligned}
S &= \frac{m}{bV_0^{n-2}} g(n) \\
t &= \frac{m}{bV_0^{n-1}} f(n)
\end{aligned}
\tag{1}
$$

Here $g(n)$ and $f(n)$ are dimensionless different functions of n which cannot be determined from the dimensional analysis. Now, let us discuss the various situations for integer values of n including zero. For $n = 0$, it is noticed from equation (1) that $t = \frac{mV_0}{b} f(0)$ and $S = \frac{mV_0^2}{b} g(0)$. Thus, both t as well as S increases with m and V_0; besides both of them decreases with b. This is

naturally expected from the usual Newton's equation of motion for a constant damping force. In such a situation, damping force becomes independent of velocity.

Hoewever, the situation looks different for $n = 1$ case. In this case, $t = \frac{mf(1)}{b}$ and $S = \frac{mV_0}{b} g(1)$. Surprisingly, $t \sim \frac{m}{b}$ and is independent of V_0. This is not correct as expected from Newton's law of motion. t in principle should grow with velocity V_0. If one has large initial speed, it is natural that there should be some non-zero time for slowing down to a smaller speed V_2. Even the equation of motion reads as $m\frac{dv}{dt} = -bv$ surely indicates the time required for the speed V_1 to V_2 ($V_2 < V_1$) is

$$
t = \frac{m}{b} \log\left(\frac{V_1}{V_2}\right)
\tag{2}
$$

How does the dimensional analysis so powerful tool in theoretical physics give a wrong result? Notice that time is proportional to a dimensionless mathematical operation of logarithmic function. In fact, it is clear from equation (2) that as $V_2 \to 0$, $t \to \infty$. In other words, given any non-zero finite speed V_1, the final speed will go to zero at an infinite time. Thus, the dimensionless function in equation (1) is indeed infinity. In fact, in such a situation, the total time is actually undefined. If we redefine the time t to slow down to some finite small speed, then we note that $t \sim \frac{mV}{b}$ indicating that t grows with V. However, the stopping distance S increases linearly with speed V_0. This is justified clearly from Newton's law

of motion $mv\frac{dv}{dx} = -bv$ indicating $S = \frac{mV_0}{b}$ consistent with the DA prediction with $g(1) = 1$.

For $n = 2$, it is found that $t = \frac{mf(2)}{bV_0}$ while $S = \frac{mg(2)}{b}$. Although in this case t depends inversely on V_0 but it is not correct. In fact, t should not decrease with speed. Newton's equation of motion clearly indicates that

$$t = \frac{m}{bV_2}\left(\frac{V_1 - V_2}{V_1}\right) \qquad (3)$$

It is evident that as $V_2 \to 0$, $t \to \infty$. This indicates that $f(2)$ will diverge to infinity. In this way one can argue that for $n \geq 2$,(there will be at least one power of V in the denominator of the expression for t) $f(n)$ must be infinite. This inherently gives a useful caution for using DA that if there is a numerical factor of the order of unity in front of the result, then DA can give correct consistent incommensurate with the physical situation. Instead if the constant turns out to be either zero or infinity, then this DA will breakdown and thus cannot be used a consistency check or prediction of the physical problems.

Is there any real relevance or importance of the equation of time in (1)? In fact, there is indeed some interesting features associated with the above equation. For example, it has been pointed out that for any given velocity V, for $n = 2$, $t = \frac{mf(2)}{bV}$, Suppose, one is interested to know the required time for an initial speed of V_i to a

final velocity V_f with $V_f < V_i$. As stated the answer will involve definitely $t = \frac{m}{bV_f} \times$ dimensionless quantity. The actual calculation in fact yields $t = \frac{m}{bV_f}\left(\frac{V_i - V_f}{V_i}\right)$ which diverges as $V_f \to 0$. The involvement of $\left(\frac{m}{bV_f}\right)$ is the key factor in describing the motion.

Now for $n = 2$, $S = \frac{g(2)m}{b}$, independent of velocity. However, intuitively speaking, the stopping distance S should depend on the speed V_0. Physically, a large initial speed V_i requires reasonably some non-zero distance to slow down to a small speed V_f. Hence, as a result, the total distance is infinite for $n \geq 2$ due to the fact that $g(n)$ is infinite. Thus, it is interesting to note that for $n \neq 1$, t and S are either both finite or infinite. For $n = 1$, the total time is infinite while the total distance turns out be finite. We invite a careful reader to investigate the damping motion of a point particle under the force $-be^{\alpha v}$ (where b and α are dimensionful constants). DA predicts that $t = \frac{m}{b\alpha}f(\alpha v)$. If one assumes $\alpha \to 0$, $f(\alpha v) \to \alpha v$, then $t = \frac{mv}{b}$. This is natural as for a constant acceleration, velocity is linearly proportional to time. The computation involving the equation of motion yields that

$$t = \left(\frac{m}{b\alpha}\right)e^{-\alpha V_f}[1 - e^{-\alpha(V_i - V_f)}] \qquad (4)$$

In the limit $\alpha \to 0$, we note that $V(t) = V_f - \frac{bt}{m}$. In the same vein, one can find out the stopping distance $S = \frac{m}{b\alpha^2}g(\alpha v)$. In the limit $\alpha \to 0$, $S \propto t^2$, a characteristic feature of particle moving under a constant acceleration. Another interesting force $F = ma_o e^{-bt}$

also requires careful analysis from dimensional approach. In such a situation $V = \frac{a_0}{b}f(bt)$ while $S = -\frac{a_0}{b^2}g(bt)$. The dimensionless functions $f(bt)$ and $g(bt)$ however to be guessed or determined from the limit $t \to \infty$.

3. Magnetic Vector Potential in Electromagnetism

We are interested to compute the vector potential ($\vec{A}$) [16] of an infinitely long straight wire carrying a uniform current I at a distance r from its axis. This problem is a standard textbook [17] one if it is asked to compute the magnetic field $\vec{B} = \vec{\nabla} \times \vec{A}$. However, we will indicate some features of this problem to another electrostatic problem of finding potential of infinitely long wire having linear charge density [18, 19, 20, 21]. In fact, this electrostatic problem is indeed a starting simple problem to understand regularization and renormalization in field theory.

To approach the problem from DA, we first note the dimensions of the following quantities which will be needed immediately. From simple basic electromagnetic theory, we find that

$$[\mu_0] = [MLT^{-2}I^{-2}]$$
$$[B] = [ML^0T^{-2}I^{-1}]$$
$$[A] = [MLT^{-2}I^{-1}] \qquad (5)$$

According to DA, by demanding $[A] =$

$[\mu_0]^x[I]^y[r]^z$, we come to the conclusion that

$$A = k\mu_0 I \qquad (6)$$

with k being a dimensionless constant. The potential in this case is completely dictated by the constant current (like the same situation for infinitely long wire having linear charge density) and is proportional directly to the current. However, the potential is independent of distance and hence, the magnetic field generated by this current vanishes. Similarly, if we now check the dependence of magnetic field on the parameters of the problem by assuming $[B] = [\mu_0]^x[I]^y[r]^z$, we note that

$$B = k_1 \frac{\mu_0 I}{r} \qquad (7)$$

with k_1 being another dimensionless constant. It is noticed clearly that the magnetic field is non-zero and varies inversely with distance. This prediction of field is however consistent with the field obtained from standard Ampere's circuital as

$$\vec{B} = \frac{\mu_0 I}{2\pi r}\hat{\phi} \qquad (8)$$

assuming the current in the $+z$ direction. Moreover, the magnetic field indeed satisfied the Maxwell's second equation namely

$$\vec{\nabla} \cdot \vec{B} = \frac{1}{r}\frac{\partial}{\partial r}(rB_r) + \frac{1}{r}\frac{\partial B_\phi}{\partial \phi} + \frac{\partial B_z}{\partial z} = 0 \quad (9)$$

indicating the absence of magnetic monopole. So, DA predicts correctly the magnetic field but not the vector potential because the constant potential gives a zero magnetic field.

So, whats going on here? Let us do a first principle calculation of the vector potential due to an infinitely long straight wire. The vector potential at a distance r from the axis of the wire can be computed as:

$$\vec{A}(r) = \frac{\mu_0 I}{4\pi} \hat{k} \int_{-\infty}^{\infty} \frac{dz}{\sqrt{r^2 + z^2}}$$
$$= \frac{\mu_0 I}{4\pi} \hat{k} \log(z + \sqrt{r^2 + z^2})|_{-\infty}^{\infty} \quad (10)$$

From the above equation (10) it is clear that $\vec{A}(r)$ diverges and is not finite. Although the vector potential is unphysical but the physically measured field $\vec{B} = \vec{\nabla} \times \vec{A} \neq \infty$. To see the independency of distance, we further move forward to obtain

$$\vec{A}(\lambda r) = \frac{\mu_0 I}{4\pi} \hat{k} \int_{-\infty}^{\infty} \frac{dz}{\sqrt{(\lambda r)^2 + z^2}}$$
$$= \frac{\mu_0 I}{4\pi r\lambda} \hat{k} \int_{-\infty}^{\infty} \frac{dz}{\sqrt{r^2 + (z/\lambda)^2}}$$
$$= \frac{\mu_0 I}{4\pi} \hat{k} \int_{-\infty}^{\infty} \frac{dt}{\sqrt{r^2 + t^2}} \quad (11)$$

where we have replaced $t = \frac{z}{\lambda}$. From the above equation (11) it is clear that the vector potential is independent of distance r as predicted by DA. A closer look at the integral equation (10) suggests that the integral is indeed scale-invariant. To see this more transparently, we rescale the argument r by a constant factor λr. Like the previous situation, a quick inspection by the substitution of $t = \frac{z}{\lambda}$ reveals the important scale invariant relation gven by

$$\vec{A}(\lambda r) = \vec{A}(r) \quad (12)$$

This means that $\vec{A}$ remains same no matter at what distance it is observed. For any two points r_1 and r_2, the potential satisfies $\vec{A}(r_1) = \vec{A}(r_2)$. This is possible if we think of a constant infinite $\vec{A}$. Although the potential is same at two points, one can still get a non-zero difference between the two infinities. Loosely speaking, we can find a unique difference between two infinities by some regularization [18, 19, 20, 21].

Let us approach this problem from another angle. To avoid the divergence at the upper and lower limits of the integral in equation (10), we put the limits to $\pm\Lambda$ accordingly and then we can consider the infinite wire (with uniform current) as a limiting case $\Lambda \gg r$. Then, the vector potential at a distance r will be

$$\vec{A}(r, \Lambda) = \frac{\mu_0 I}{4\pi} \hat{k} \int_{-\Lambda}^{\Lambda} \frac{dz}{\sqrt{r^2 + z^2}}$$
$$= \frac{\mu_0 I}{2\pi} \hat{k} \int_{0}^{\Lambda} \frac{dz}{\sqrt{r^2 + z^2}}$$
$$= \frac{\mu_0 I}{2\pi} \hat{k} \log\left(\frac{\Lambda}{r} + \sqrt{1 + \frac{\Lambda^2}{r^2}}\right) \quad (13)$$

Moreover, the vector potential in equation (13) does indeed satisfy the Coulomb gauge condition

$$\vec{\nabla} \cdot \vec{A} = \frac{1}{r}\frac{\partial}{\partial r}(rA_r) + \frac{1}{r}\frac{\partial A_\phi}{\partial \phi} + \frac{\partial A_z}{\partial z} = 0 \quad (14)$$

since A_z is independent of z. It is evident that the potnetial is finite everywhere so long as the cut-off is finite.Thus, the finiteness of the potential is rendered by the upper-cutoff used in the first principle calculation. Now, if we calculate the magnetic field from the relation $\vec{B} = \vec{\nabla} \times \vec{A} = -\hat{\phi}\frac{\partial A_z}{\partial r}$

appropriate to the cylindrical symmetry of the problem, then we obtain

$$\vec{B} = -\hat{\phi}\,\frac{\mu_0 I}{2\pi}\left(\frac{1}{\Lambda + \sqrt{\Lambda^2 + r^2}}\frac{r}{\sqrt{\Lambda^2 + r^2}} - \frac{1}{r}\right) \quad (15)$$

Note that a real wire has a finite length and as a result, the vector potential as well as the magnetic field is finite at any distance.

The presence of this cut-off Λ however breaks the translational symmetry of the original problem along the axis of the wire. The vector potential is not invariant under the transformation $r' \rightarrow r + c$ as can be easily from the above equation (13).

For large cut-off ($\Lambda \gg r$), one can approximate the argument of the logarithm function to obtain

$$\begin{aligned}\vec{A}(\Lambda, r) &\approx \frac{\mu_0 I}{2\pi}\,\hat{k}\log\left(\frac{2\Lambda}{r}\right)\\ &= -\frac{\mu_0 I}{2\pi}\,\hat{k}\log\left(\frac{r}{r_0}\right)\\ &\quad+\frac{\mu_0 I}{2\pi}\,\hat{k}\log\left(\frac{2\Lambda}{r_0}\right)\end{aligned}$$

$$(16)$$

Thus we see that the magnetic vector potential in the vicinity of a straight wire is a vector field parallel to the wire. For infinite length of the wire the magnetic vector potential turns out to be infinite. However, for a finite length, the vector potential given *exactly* by equation (13) is finite. For finite length resembling close to long infinie wire, the vector potential is approximated by equation (16). We have written the formula of the vector potential in a form

$\frac{\mu_0 I}{2\pi}F(\Lambda r)$. It turns out from the computation that $F(\Lambda r)$ has the dimensionless logarithm function. This is precisely the reason for not obtaining the explicit dependence of distance. We have introduce a lengthscale r_0 to set the zero of the vector potential $\vec{A}$. Thus, the reason for the infinity in $\vec{A}$ as $\Lambda \rightarrow \infty$ is that we have tried to set $\vec{A}(\infty) = 0$. This is not possible when the current distribution itself extends to infinity. For the boundary condition $\vec{A}(r) \rightarrow 0$ as $r \rightarrow \infty$ is essentially valid for the localized current distribution in a finite regime (in particular the current density $\vec{J}(r)$ must fall off faster than $\frac{1}{r}$ as $r \rightarrow \infty$). This is reminiscent of the electrostatic potential [18, 19, 20] of an infinite long straight wire uniformly charged with charge p per unit length given by

$$\phi(p, \rho) = \frac{p}{2\pi\epsilon_0}\log\left(\frac{2\Lambda}{\rho}\right) \quad (17)$$

And in the same limit ($\Lambda \gg r$), from equation (15) the physically observable magnetic field is given by

$$\vec{B} = \hat{\phi}\,\frac{\mu_0 I}{2\pi r} \quad (18)$$

and is consistent with the result computed even from the equation (16). The vector potential is formally infinite as $\Lambda \rightarrow \infty$, however the physically observable quantity being the magnetic field should be independent of cutoff Λ and finite at all points. In fact as long as the vector potential has the form given by equation (16), the magnetic field is finite and given by the equation (18).

Is there a simple way to understand the logarithmic function appearing in the equation (16)? This can be visualized in the following way from the scale invariant equation (12). With the restriction on the form of the vector potential satisfying equation (12), it is easy to frame the differential equation for A as

$$r\frac{\partial A(\lambda r)}{\partial \lambda} = 0$$

$$\lambda \frac{\partial A(\lambda r)}{\partial r} = A'(r)$$

$$z\frac{\partial^2 A}{\partial z^2} + \frac{\partial A}{\partial z} = 0 \qquad (19)$$

with $z = \lambda r$ as the dimensionless variable. The equation (19) has a generic solution given by $A(z = \lambda r) = \log(\lambda r)$.

Essentially, the reference point is the key in this particular problem, It is shown and argued clearly that the reference point *cannot* be taken at infinity (i.e. $\vec{A}(r) \neq 0$ at $r \to \infty$). In fact there is a point (r_0) between zero and infinity where the vector potential indeed vanishes. A careful look into the problem reveals that the current distribution is not confined to a finite region. That's why the potential cannot go to zero at infinity. A better way of treating this type of problem is through the appropriate differential equation for the vector potential in a finite domain having cylindrical symmetry [22].

3.1 Computation of Vector Potential From the Field

In the previous section we have computed the magnetic field from the vector potential.

Is it possible to compute the vector potential from the magnetic field uniquely? Note that due to gauge transformation, one can always add some gradient of a smooth function $\chi(r, t)$ to obtain the same magnetic field ($\vec{A}' = \vec{A} + \vec{\nabla}\chi$, $\vec{B}' = \vec{\nabla} \times \vec{A}' = \vec{B}$). Since, the field $\vec{B}$ possesses only the ϕ component, therfore, the relevant ϕ component of the cylindrical curl is required for the computation of the vector potential. Hence, the necessary first order partial differential equation for the potential will be

$$\frac{\partial A_r}{\partial z} - \frac{\partial A_z}{\partial r} = \frac{\mu_0 I}{2\pi r} \qquad (20)$$

Moreover, the symmetry of the problem clearly indicates that $\vec{A}$ cannot be a function of z since the current carrying wire is uniform with z. Therefore, we have a simple equation given by

$$-\frac{\partial A_z}{\partial r} = \frac{\mu_0 I}{2\pi r} \qquad (21)$$

with the solution

$$A_z = -\frac{\mu_0 I}{2\pi} \log r + C \qquad (22)$$

The integration constant C needs the appropriate boundary condition for this particular problem as mentioned earlier. In fact, if we choose the zero reference of A_z at $r = r_0$, then we eventually get the correct expression for z component of the the vector potential as

$$A_z(r) = -\frac{\mu_0 I}{2\pi} \log\left(\frac{r}{r_0}\right) \qquad (23)$$

consistent with the first term in equation (16). However, we can always add some

constant with the above function of $A_z(r)$ (as is done through the second term in equation (16)) which can give the same magnetic field. In other words, one can always add any vector with zero curl without altering the magnitude of the magnetic field. Thus, the uniqueness of the vector potential is not restored from this formulation.

3.2 Field and Potential Inside a Cylindrical Wire

We are interested to comment on the vector potential inside the cylindrical wire of radius R. Because of the presence of this extra length scale R, we propose the vector potential and the corresponding field should depend on the parameters in the following way

$$[A] = [\mu_0]^x [I/R^2]^y [r]^z$$
$$[B] = [\mu_0]^p [I/R^2]^q [r]^s \qquad (24)$$

Thus. DA predicts the variation of the potential and the field as

$$A = \left(\frac{\mu_0 I}{R^2}\right) r^2$$
$$B = \left(\frac{\mu_0 I}{R^2}\right) r \qquad (25)$$

showing the finiteness at any point. Again computation via Ampere's circuital law yields

$$\oint \vec{B} \cdot d\vec{l} = \frac{\mu_0 I r^2}{R^2}$$
$$\vec{B} = \frac{\mu_0 I}{2\pi R^2} r \, \hat{\phi} \qquad (26)$$

consistent with the DA prediction. Since the magnetic field is along the azimuthal direction we can now obtain the vector potential from the equation

$$\frac{\partial A_r}{\partial z} - \frac{\partial A_z}{\partial r} = \left(\frac{\mu_0 I}{2\pi R^2}\right) r \qquad (27)$$

Again, the wire being long enough, there cannot be a variation with respect to z. Thus the only non-zero component of the vector potential should satisfy

$$-\frac{\partial A_z}{\partial r} = \left(\frac{\mu_0 I}{2\pi R^2}\right) r \qquad (28)$$

The solution of the above equation (28) is identified as

$$\vec{A}(r) = -\left(\frac{\mu_0 I}{4\pi R^2}\right) r^2 \, \hat{z} \qquad (29)$$

consistent with the DA result shown above. Thus, in this case there is no breakdown of DA to compute the field as well as the vector potential. Besides, like previous situation, $\vec{\nabla} \cdot \vec{B} = 0$ and Coulomb gauge $\vec{\nabla} \cdot \vec{A} = 0$ are indeed satisfied.

4. Critical Phenomenona in Statistical Mechanics

In this section, we would like to present a situation of violation of DA in equilibrium statistical mechanics namely in critical phenomena and phase transition [23, 24]. Landau theory of critical phenomena [25] starts with an effective theory (Φ^4) with a fluctu-

ating field Φ in an external magnetic field h

$$
H_{eff}[\Phi] = \int \left[\frac{1}{2}(\nabla\Phi)^2 + \frac{1}{2}r_0\Phi^2 \right.
$$
$$
\left. + \frac{1}{4}u_0\Phi^4 - h\Phi \right] d^d x
$$
$$(30)$$

The partition function of this system is defined as

$$
Z = \int [D\Phi] \, e^{-H_{eff}[\Phi]} \qquad (31)
$$

From the above two definitions, we can easily find out the dimensions of the parameters in the above model Hamiltonian. Since, H_{eff} is dimensionless, then the dimension of $[\Phi] = L^{1-\frac{d}{2}}$ subsequently, it is easy to notice that

$$
[r_0] = [L]^{-2}
$$
$$
[u_0] = [L]^{d-4}
$$
$$
[h] = [L]^{-\frac{2+d}{2}} \qquad (32)
$$

Again from phenomenological ground, it is assumed that $r_0 \propto (T - T_c)$, where T_c denotes the critical transition temperature. Now, the two point correlation function is defined as

$$
G(\vec{r} - \vec{r}') = \left\langle \Phi(\vec{r})\Phi(\vec{r}') \right\rangle
$$
$$
= \frac{\int [D\Phi] \, e^{-H_{eff}[\Phi]}\Phi(\vec{r})\Phi(\vec{r}')}{\int [D\Phi] \, e^{-H_{eff}[\Phi]}} \qquad (33)
$$

Physically speaking, $G(\vec{r} - \vec{r}')$ provides one a direct measure of the influence of the leading microscopic fluctuations of the order parameter present at $\vec{r}$ on the behavior at $\vec{r}'$ in the system. Using the dimension of Φ, we find the dimension of $G(\vec{r} - \vec{r}')$ as $[L]^{d-2}$. However, experimental observations suggest that at the critical transition temperature T_c, the correlation function at any arbitrary dimension d varies with distance as power law exponent η defined as:

$$
\left\langle \Phi(\vec{0})\Phi(\vec{r}) \right\rangle \sim \frac{1}{|\vec{r}|^{d-2+\eta}} \qquad (34)
$$

It is noticed that naive engineering dimensional analysis agrees with $\eta = 0$ irrespective of any spatial dimension but the experimental data reveal the non-zero finite value (for example $\eta = \frac{1}{4}$ for 2d Ising model). Thus, the non-zero value of η in Landau theory seems to violate the naive DA. In fact, the prediction $\eta = 0$ typically results from the neglect of fluctuations in mean field theory.

In other words, we can correct this through some another length scale L such that $G(\vec{r} - \vec{r}')$ must have a dimension $L^{-\eta}$ to save the principle of homogeneity in equation (34). A careful study however indicates that the violation originates from another length scale in the problem apart from only and one correlation length ξ as defined in the phase transition. The most important correlation length $\xi \sim r_0^{-1/2}$ diverges at the temperature approaces T_c. For example, the microscopic length scale such as lattice spacing a or some cut-off in the original problem must be included in the dimensional analysis. However, close to the critical point, the nicroscopic length scale can be ignored because of the emergnece of the infinite correlation lenth ξ. This is not only the length

scale in the problem and there may be other relevant length scales *equally important* in such situation. In fact, physics *at all length scales* needs to be undertaken to understand the critical behavior and exponents in the phase transition. Note that power-law dependence on distance implies that there is no length scale inherent in the system and hence, a scale invariance is noticed. If one allows $r \to r' = br$ alongwith $\Phi \to \Phi' = b^\omega \Phi$, then we easily notice from (34) that the scale invariancy is restored only if $\omega = \frac{d-2+\eta}{2}$. The factor b thus drops out from the both sides of the equation (34). The non-zero value of η and this breakdown can be handled in the framework of renormalization group along with valid scaling theory[23].

5. Conclusion

In this article we have presented few examples from classical mechanics, electrodynamics and critical phenomenon where the breadown of DA occurs. We have pointed out the reason for such breakdown of this wonderful technique in theoretical physics. The three problems presented here share essentially some common divergences in their parameters. If the dimensionless factor involving some parameters in course of DA is of the order of unity, then DA will be able to give correct consistent prediction incommensurate with the physical situation. Instead if the dimensionless factor turns out to be either zero or infinity, then this DA will breakdown and thus cannot be used a con-

sistency check or prediction of the physical problems.

Acknowledgments

References

[1] G. I. Barenblatt, *Dimensional Analysis*, (Gordon Breach Science Publishers, New York, 1987).

[2] Q. M. Tan, *Dimensional Analysis*, (Springer-Verlag, Berlin Heidelberg, 2011)

[3] A. A. Sonin, *The Physical basis of dimensional analysis*, (Department of mechanical engineering, MIT, Cambridge, second edition, 2001).

[4] G. I. Barenblatt, *Scaling, Self-similarity, and Intermediate Asymptotics*, (Cambridge University Press, Cambridge, UK, 1996)

[5] Tatjana Misic, Marina Najdanovic-Lukic and Ljubisa Nesic, *Eur. J. Phys.*, **31**, 893 (2010).

[6] G. B. West and J. H. Brow, *Phys Today*, **57**, 36 (2004).

[7] D. Jana, *Dimensional Analysis: Modern Perspectives*, (Lambert Academic Publishing, Germany, 2011).

[8] W. H. Press, *Am. J. Phys.*, **48**, 597 (1980).

[9] S. Vogel, *Phys. Today*, **51**, 22 (1998).

[10] F. Felber, *Phys. Today*, **52**, 11 (1999).

[11] Knut Schmid-Nielsen, *Scaling: Why Animal Size is So Important* (Cambridge University Press, Cambridge, England, 1984).

[12] D. Jana, *Phys. Edu.*, **32**, Jan-Mar, Issue 1, Article No. 1 (2016).

[13] D. Jana, *Phys. Edu.*, **25**, 35 (2008).

[14] D. Jana, *Phys. Edu.*, **19**, 167 (2002).

[15] David Morin, *Introduction to Classical Mechanics with problems and solutions*, (Cambridge University Press, 2008).

[16] D Iencinella and G Matteucci, *Eur. J. Phys.*, **25**, 249 (2004).

[17] D. J. Griffiths, *Introduction to Electrodynamics* 3rd edn (Upper Saddle River, NJ: Prentice-Hall, 1999).

[18] T. Padmanabhan, *Resonance*, June, 510 (2008).

[19] M. Hans, *Am. J. Phys.*, **51**, 694 (1983).

[20] C. Kaufman, *Am. J. Phys.*, **37**, 560 (1969).

[21] F. Oldness and R. Scaliest, *Am. J. Phys.*, **79**, 306 (2011).

[22] J. L. Jimenez, J. Campos and JAE Roa-Neri, *Euro. J. Phys.*, **33**, 467 (2012).

[23] N. Goldenfeld, *Lectures on Phase transitions and the Renormalization Group*,(Addison-Wesley Publishing Company, New York, 1992).

[24] S. M. Bhattacharjee, *Critical Phenomena: An Introduction from a modern perspective*, ArXiv: cond-mat/0011011v1.

[25] P. C. Hohenberg and A. P. Krekhov, *An introduction to the Ginzburg-Landau theory of phase transition and non-equilibrium patterns*, ArXiv. 1410.7285v3

Understanding Clipping Circuits Finely

Prabhjeet Kaur Dhillon

Department of Basic Sciences,
Guru Nanak College for Girls,
Sri Muktsar Sahib, India
E-mail: prabhjeetdhillon@gmail.com

Abstract

Clipping circuits which help in removing positive or negative part of waveform are often found difficult to understand when it comes to analysing the circuit and predicting the output waveform. Learning is enhanced only if the circuits are analysed critically. This article analyses clipping circuits in depth and suggests creative ways to understand them.

Keywords: clipping, transition voltage

1. Introduction

Performing electronics experiments is a challenging task, considering the fact that if you happen to make wrong connection you can even end up shorting a component. So if we analytically perform electronics experiments the probability of making a faulty connection reduces drastically. One such undergraduate electronics experiment is that of a clipping circuit. A clipper is a circuit that removes either positive or negative parts of a waveform.[1]

Depending on whether diode is connected in series or in shunt position it is called series or shunt clipper respectively. Further if external battery supply is applied it is called a biased clipper. Now the question arises how to make students understand clippers profoundly?

2. Positive and Negative Clipper

First we start with basics to that of differentiating between a positive and a negative clipper. If the positive half of signal is clipped then it is called positive clipper and if the signal's ngative half is clipped then it is called negative clipper. Further whether the diode is connected in series or in parallel with the output the clipper is called series or shunt clipper respectively.

If we only ask students which half of the signal is clipped to understand whether it is a positive clipper or a negative clipped we will be lacking in providing them an insight. We should ask students instead to simultaneously observe both input and output waves so that they can observe the effect of using the circuit on input wave. Ask them to compare peak to peak voltages and also the time period. Amplitude of input

and output signal (Fig. 1(b)) is 1V and time period is 1ms. This will help them in a better visualisation of both signals.
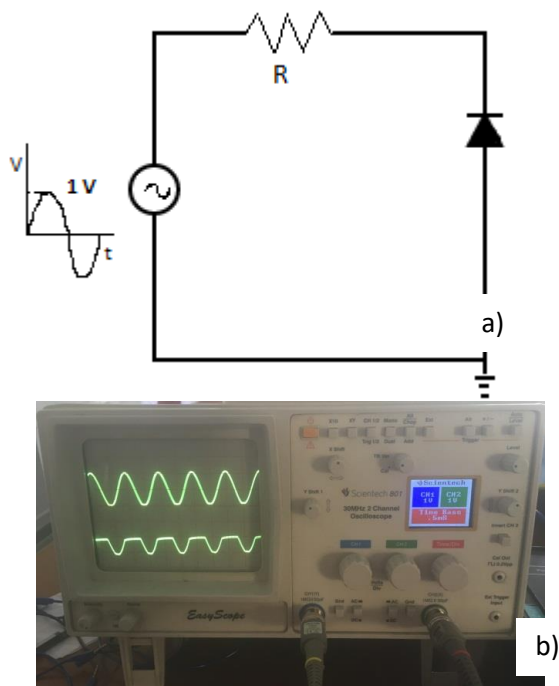
Fig. 1 Shunt positive clipper a) Circuit diagram b) Output waveform

Similarly diode connected in opposite direction in Fig1a) will form shunt negative clipper. Alternatively when the diode is connected in series with the output it will form series positive or negative clipper depending upon in which direction diode is connected. Comparison of all waveforms will help us in understanding all four types of clippers profoundly, the simplest means being comparing the amplitude, time period and pattern of waveform.

3. Biased Clipper

A biased clipper is one in which an external power supply controls the shape of output wave[2]. Depending upon whether a positive or negative power supply is given to the diode, output signal will be cut accordingly. For biased waveform before looking at the output waveform students should be able to predict the results. For this the transition voltage is the key factor[2]. Here transition voltage is the voltage supplied externally to the diode circuit. Fig.2 shows a biased clipper with 5 V input signal. Here the external supply of V Volts competes with the input signal of 5 Volts amplitude. Whether the diode will be in ON or OFF

state will be determined by the competition between the two.
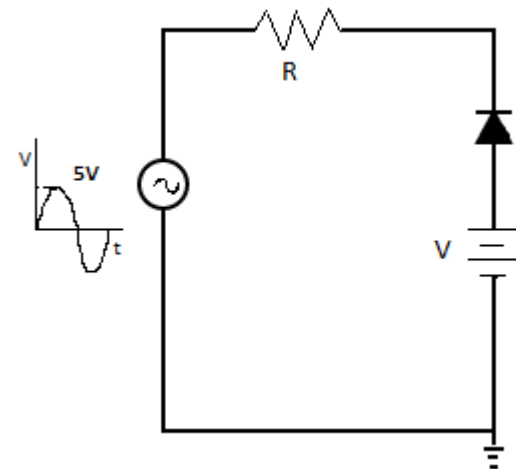
Fig. 2 Biased clipper with 5V input signal

Here V Volts is transition voltage. For positive half cycle, if input voltage v_i is greater than V Volts the diode will be in OFF state and if v_i is less than V Volts then diode will be in ON state. For negative half cycle the diode will be in ON state. In ON state diode will be conducting and for the case of ideal diode with zero potential drop it will act as short circuit and output will be V Volts. During OFF state diode will act as open circuit and the entire signal will appear as it is at the output. Figure 3 shows output of circuit in Fig.2.Here the input and output waves are superimposed to have a clear picture of clipping output and simultaneously compare it with input. Here a sinusoidal input wave is taken with amplitude of 5V. External supply is taken to be 1V, 2V and 3V respectively for the three cases. Accordingly the output wave shifts by 1V in each case.
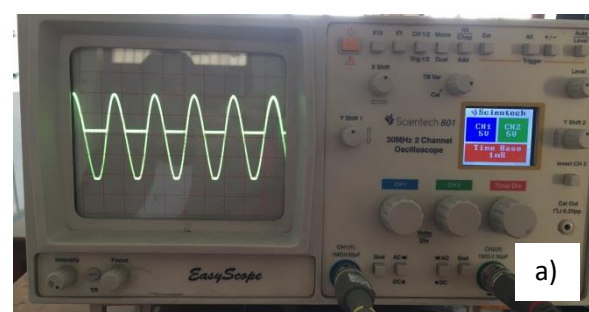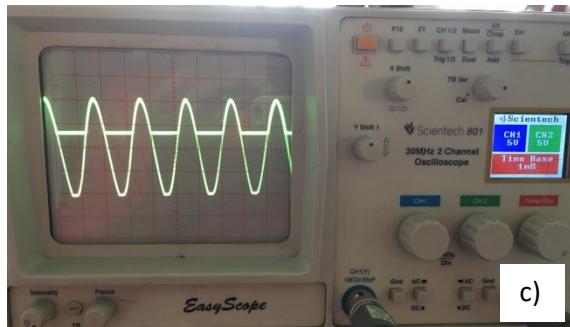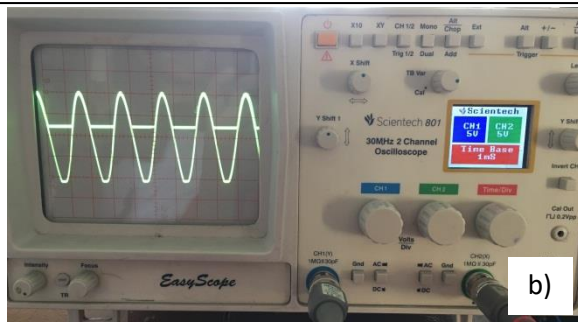
Fig. 3 Output waveforms of a biased clipper circuit (Fig. 2) with input voltage of amplitude 5 V and external supply of a) 1V b) 2V c) 3V.

4. Conclusion

Analysis of circuit and waveform profoundly helps in a better understanding of clipping circuits. Creativity in teaching electronic circuits enhances learning experience and makes it easy.

References

[1]Malvino A and Bates D J Electronic Principles, 7th edition, Tata McGraw Hill Education Private Limited.

[2]Boylestad R L and Nashelsky L Electronic Devices and Circuit Theory 10th edition Pearson.

[3]DeHaan R L 2011 *Science* **334** 1499-500